Active Fluids
Notes prepared for the 2026 Boulder School:
Geometry and Topology in Soft Matter Physics

M. Cristina Marchetti[1]

[1] *Department of Physics, University of California Santa Barbara, Santa Barbara, CA 93106, USA*

CONTENTS

I. PREAMBLE

This set of notes is a somewhat biased summary of a very broad field of rapidly evolving research. It does not not claim to be complete nor free of typos. It does not contain a complete and historically accurate set of citations which can be found in the cited review articles, and it is not intended for outside distribution.

I will probably only cover part of these notes in the lectures. Suggested exercises can be found throughout.

There are several review articles on the topics covered in these lectures and on active matter in general that I encourage you to consult.

- For a general, technical and comprehensive review of the field of active matter, even if now a little dated, see Ref. [1].
- For a "review of reviews" that provides many useful references see Ref. [2].
- For a short review of Active Brownian Particles, see Ref. [3]. For a review of MIPS, see Ref. [4]. For a more comprehensive review of scalar active matter, see Ref. [5].
- For a very broad-strokes overview of active nematic liquid crystals, see Ref. [6].
- For a review of synthetic active nematic liquid crystals, especially the microtubule-kinesin nematic liquid crystal engineered in 2012 by Zvonimir Dogic [7] that effectively started the field of active nematics, see Ref. [8].
- For brief reviews of the relevance of nematic order and topological defects to biology, see Refs. [9] and [10].
- For a recent review on defects and topological phenomena in active matter, see Ref. [11]

Part of these lecture notes were prepared with help by Sofia Marchioretto.

II. ACTIVE MATTER: A BRIEF INTRODUCTION

The name active matter refers to collections of entities that individually consume free energy to generate motion and forces [1, 12]. Through interactions, these "active particles" (e.g., bacteria, phoretic colloids, living cells, humans) spontaneously organize in emergent large-scale structures with a rich range of behaviors. The defining property of an active system is that the energy input that maintains the system out of equilibrium, whether truly internal or created by contact with a proximate surface, acts individually and independently on each active particle [13].

It is important to note that once the chemo-mechanical processes that convert fuel into motion are integrated out, the dynamics of active particles breaks time reversal symmetry (TRS) in a *local* and sustained manner. This breaking of TRS should be contrasted with more conventional nonequilibrium systems that are displaced from equilibrium *globally* by an external force that picks out a direction in space, such as an electric field, or as in sedimentation under gravity, or are forced at the boundaries, such as through an imposed mechanical shear. Due to the breaking of TRS at the microscale, active systems do not obey detailed balance and can generate self-sustained flows and cyclical currents. Thus, steady-state movies of active dynamics run forwards and backwards do not look the same, as they would in Newtonian mechanics.

Another important property of active system is that, in contrast to, say, sedimenting particles, the forces at play are always internal, hence the dynamics of active particles is "force free". Non-reciprocal interactions that evade Newton's Third Law of action-reaction are ubiquitous in active and living systems that break detailed balance at the microscale. Examples include social forces, promoter-inhibitor couplings among cell types in developing organs and organisms, antagonistic interspecies interactions in bacteria and prey-predator systems. Effective nonreciprocal interactions arise when partciles are immersed in a nonequilibrium medium that mediates the intercations, as in dusty plasma or phoretic active colloids.

There are now many reviews focusing on different aspects of active matter [14–17], a few books, and even a "review of reviews" that classifies various review articles [2]. The present review specifically focuses on continuum theories of active nematic liquid crystals. Nematic order has been observed ubiquitously in active and living systems, and the framework described below has been proven useful in a variety of settings. This review is intended to provide a pedagogical introduction for students entering the field. It therefore starts with a brief summary of those aspects of liquid crystal physics that are needed to approach the study of active nematics. While these topics can be found in standard texbooks, we feel it is useful to summarize them here before moving on to the study of active systems. We then introduce active nematic hydrodynamics and employ it to describe a number of phenomena that have been observed across diverse physical realizations. We also include a brief section on ongoing work on active elasto-nematics. Finally we conclude with some comments on future directions [16].

A. Examples of active systems

To introduce active matter, we first need to define an "active particle". For concreteness, let us consider a specific example: bacteria. For instance, *E.coli* is a rod-shaped bacterium with a body about $2-3\mu m$ long and $0.5\mu m$ in diameter and a long tail of flagella that allows it to swim [18]. It composes about 1% of the gut flora. An individual *E. Coli* swims through run-and-tumble: It travels in a straight line at a speed of $10-30\mu m/s$ and every second or so it spreads out its flagella and undergoes a tumble, i.e., a large change in direction [19]. At times large compared to the tumble rate, the dynamics is diffusive, but this is not a conventional Random Walk. A dense *E. Coli* suspension exhibits coordinated motion and spontaneous organization at large scales:
- It behaves like a self-flowing fluid: in a nutrient-rich medium one observes a characteristic swarming dynamics named bacterial turbulence.
- When starved, *E.Coli* self-organizes in a variety of patterns, such concentric rings of high and low bacterial density or regular arrays of spots of high cell density.
- It can form solid-like biofilms.

There are many other examples spanning a broad range of scales, including:

- Organization of chromatin inside the cell nucleus;
- Structures in the cell interior, such as the cytoskeleton that control cell mechanics and motility and the mitotic spindle that drives cell division and chromosome separation;
- Multicellular systems: biological tissue, wound healing, development
- Insects, fish, birds, people
- Collections of robots

- Phoretic colloids, engineered microswimmers

- Reconstituted suspensions of motor proteins (myosins, kinesins) and cytoskelatal filaments (F-actin, microtubules).

B. Classes of active matter

Active systems spontaneous organize in a variety of collective phases with properties and behavior controlled by the symmetry of both the active "particles" and their interactions. Four important classes are [1, 17]:

- *Scalar active matter.* Spherical active particles (e.g., colloids driven by a variety of phoretic effects) with radially symmetric interactions and no alignment can undergo motility induced phase separation (MIPS) in the absence of any attractive interactions. We will not cover this topic here, but see Refs [3, 4]. This is called scalar active matter because the order parameter that describes the transition is the density difference between the dilute and the dense phases, hence a scalar. A local number density field can be defined as

$$\rho(\mathbf{r},t) = \Big\langle \sum_n \delta(\mathbf{r}-\mathbf{r}_n(t)\Big\rangle \,, \tag{1}$$

  where $\mathbf{r}_n$ is the position of the n-th particle and the brackets denote an average over a local patch centered at $\mathbf{r}$.

- *Polar active matter.* Active particles with a head and a tail, such as many bacteria, birds or fish, are polar and can organize in states with polar order quantified by a vectorial order parameter. This can be defined as a polarization density field in terms of unit vectors $\boldsymbol{\nu}_n$ identifying the polarization of each unit,

$$\mathbf{p}(\mathbf{r},t) = \Big\langle \sum_n \boldsymbol{\nu}_n \delta(\mathbf{r}-\mathbf{r}_n(t)\Big\rangle \,. \tag{2}$$

  An example is flocking agents where the polarization (up to a factor of propulsive speed) is also the mean velocity of the flock. Polar active particles can also antialign, in which case they may organize in a state with nematic (apolar) order.

- *Nematic active matter* Apolar active particles have no head and tail and exert force dipoles on their surroundings. Examples are microtubule-kinesin bundles and melanocytes, the cells that shake the pigment in our skin. They can organize in states with uniaxial nematic order, which is quantified by a tensorial order parameter (arank-2 traceless tensor - see below for explanation), defined as

$$Q_{ij}(\mathbf{r},t) = \frac{1}{\rho}\Big\langle \sum_n \left(\nu_{ni}\nu_{nj} - \frac{1}{d}\delta_{ij}\right)\delta(\mathbf{r}-\mathbf{r}_n(t)\Big\rangle \,, \tag{3}$$

  where d is the dimensionality of the system. Here and below $i, j, k, ...$ are used for Carthesian components.

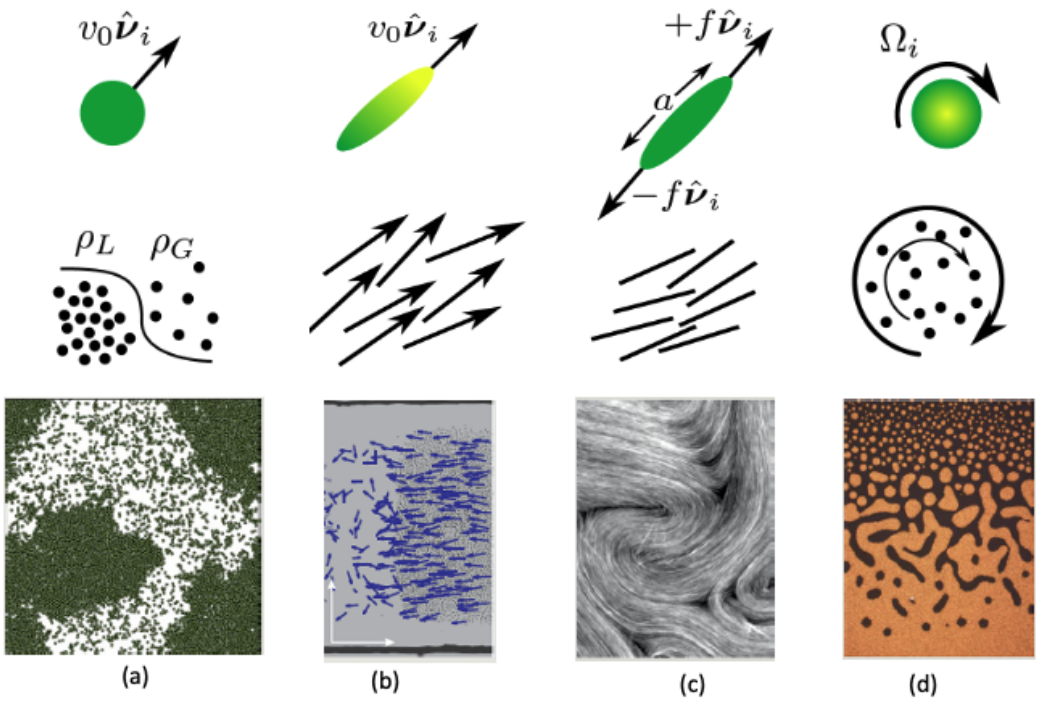

Figure 1. Various classes of active matter. (a) Scalar active matter composed of isotropic particles self-propelled at speed v_0 along an axis $\hat{\boldsymbol{\nu}}_i$ that undergo MIPS. (b) Polar active matter composed of selfpropelled polar aligning active particles that undergo a flocking transition. (c) Nematic active matter of eleongated particles that extert force dipoles on their environment. (d) Chiral active matter composed of particles that self-spin at a rate Ω_i in two dimensions. The images in the bottom row are, from right to left: MIPS in a fluid of active Brownian particles (adapted from Ref. [3]); a flock of colloidal polar particles (adapted from Ref. [20]); a microtubule-kinesin active nematic (adapted from Ref. [7]); a fluid of colloidal spinners (adapted from Ref. [21]).

- *Chiral active matter.* Active particles may be chiral and organize in states with microscopic chirality. An example are colloidal spinners in a fluid. In two dimensions, chirality is captured by a psuedoscalar that quantifies the rotation frequency and can be deifned as

$$\Omega(\mathbf{r},t) = \left\langle \sum_n \Omega_n \delta(\mathbf{r}-\mathbf{r}_n(t)\right\rangle , \tag{4}$$

  wher Ω_n is the spinning rate of particle n.

This is not an exhaustive list. For instance, it is of course possible to have chiral polar and chiral nematic states, as well as active solids that can exhibit translational order.

C. A bit of history of the field

In 1995 the Hungarian physicist Tamás Vicsek proposed a minimal model of bird flocking inspired by the physics of magnetism [22]. He showed that a collection of flying spins - self-propelled point particles traveling with fixed speed in a direction updated by alignment with neighbors in a noisy environment - can undergo a phase transition from a disordered state where the spins fly randomly in all directions to an ordered state of collective motion. Just a few months later, Vicsek presented his work in a seminar at IBM Yorktown Heights. John Toner and Yuhai Tu realized that they could turn Vicsek's agent-based model into a field theory and formulated what are now known as the Toner-Tu equations of flocking [23].

Truth be told, what physicists now know as the Vicsek model had effectively been previously formulated by Craig Reynolds, a computer scientist working for the animation industry, who in 1986 created *Boids* [24] – an agent-based simulation of collective motion that he employed, for instance, to generate the animation of flying bats in the 1992 feature *Batman Returns*. Indeed the model appears even earlier in the literature, in theories of fish schools by Aoki [25] and Partridge [26]. While these contributions remained unnoticed by the physics community for some years, Reynolds, a leader in the development of three-dimensional animation, was awarded a Scientific and Technical Award by the Academy of Motion Picture Arts and Sciences in 1998. In the intervening years, the notion introduced by Vicsek that the collective dynamics of self-driven entities can be described as a nonequilibrium phase transition gained enormous popularity among physicists and was shown to provide a powerful framework for describing spontaneous organization on many scales. For their key contribution to the creation of the field of active matter, Vicsek, Toner and Tu received the Lars Onsager prize of the American Physical Society in 2020.

The first published use of the term Active Matter appears to be in Ref. [27]. Active Membranes appear a little earlier in the physics literature [28, 29]. The term "active" in reference to fuel-driven transport across a membrane, against a concentration gradient, is standard in biology [30]. Active stresses in a fluid medium suffused with sustained energy conversion make their first appearance in Ref [31].

III. ACTIVE DYNAMICS VERSUS BROWNIAN DYNAMICS

To understand the key role of motility in driving self-organization, it is useful to begin by contrasting the dynamics of an active or self-propelled particle to that of a familiar Brownian particle. At least three types of active dynamnics are commonly considered in the literature: Active Brownian Particles (ABPs), Active Ornstein-Uhlenbeck Particles (AOUPs), and Run-and-Tumble Particles (RTP). Here we will mainly focus on ABPs and briefly mention the connection to this other commonly considered dynamics. A comprehensive review can be found in Ref. [14].

A. Brownian motion

Let us start with a brief summary of how we describe Brownian motion - the herratic motion of a colloidal particle of mass m in a fluid in thermal equilibrium at temperature T. An excellent description of Brownian morion can be found in Ref. [32]. We write a stochastic equation of motion

or Langevin equation for the velocity $\mathbf{v}$ of the particle as

$$m\frac{d\mathbf{v}}{dt} = -\gamma\mathbf{v} + \mathbf{f}(t) \; . \tag{5}$$

The right hand side of Eq. (5) represents the forces due to the fluid. The first term is the mean drag from the surrounding fluid. The second term represents the random kicks that the colloid receives from collisions with fluid molecules that drives the motion of the Brownian particle. The effect of such collisions is modeled as a stochastic force with Gaussian distribution and zero mean, i.e.,

$$\begin{aligned} \langle \mathbf{f}(t) \rangle &= 0 \; , \\ \langle f_i(t) f_j(t') \rangle &= 2\Delta\delta_{ij}\delta(t-t') \; , \end{aligned} \tag{6}$$

where i, j denote Carthesian components and the variance Δ will be determined by requiring the Brownian particle to be in thermal equilibrium with the fluid at long times. The $\delta(t)$ correlations of the random forces corresponds to the assumption that successive kicks/collisions are uncorrelated in time. Note that this equation contains a characteristic time scale $\tau = m/\gamma$ that represents the relaxation time of the mean velocity, $\langle \mathbf{v}(t) \rangle = \mathbf{v}(0)e^{-t/\tau}$. Importantly, here the equilbrium ambient fluid generates both the dissipation and the drive. Since we have in mind a micron-size colloid, the drag or friction coefficient γ can be calculated in the low Reynold number limit. For a spherical particle of radius R in $3D$ it is given by the Stokes expression $\gamma = 6\pi\eta R$, where η is the shear viscosity of the fluid.

To determine Δ, we formally integrate Eq. (5). Assuming for simplicity $\mathbf{v}(0) = 0$, we find

$$\mathbf{v}(t) = \frac{1}{m}\int_0^t dt' e^{-(t-t')/\tau}\mathbf{f}(t') \; . \tag{7}$$

It is then easy to show that

$$\langle |\mathbf{v}(t)|^2 \rangle = \frac{\Delta}{m\gamma} d\left(1 - e^{-2t/\tau}\right) \; . \tag{8}$$

We require that at long time ($t \gg \tau$) the Brownian partcile be in thermal equilibrium with the fluid. This means that $\langle |\mathbf{v}(t\to\infty)|^2 \rangle$ must be the equilibrium value from equipartition $\langle |\mathbf{v}(t)|^2 \rangle_{eq} = d\frac{k_B T}{m}$. This gives

$$\Delta = \gamma k_B T \; . \tag{9}$$

The dynamics of Brownian particles is generally quantified in terms of the Mean-Square Displacement (MSD). This is easily obtained from the Langevin equation as

$$\langle [\mathbf{r}(t) - \mathbf{r}(0)]^2 \rangle = 2d\frac{k_B T}{\gamma}\left[t - \tau\left(1 - e^{-|t|/\tau}\right)\right] \; . \tag{10}$$

It is useful to consider two limiting cases of this expression. Letting $\Delta\mathbf{r} = \mathbf{r}(t) - \mathbf{r}(0)$, we find

$$\langle [\Delta\mathbf{r}]^2 \rangle = \begin{cases} d\frac{k_B T}{m} t^2 & \text{for} \quad t \ll \tau \quad \text{ballistic} \\ \\ 2dDt & \text{for} \quad t \gg \tau \quad \text{diffusive} \end{cases} \tag{11}$$

where

$$D = \lim_{t\to\infty} \frac{\langle [\Delta \mathbf{r}(t)]^2 \rangle}{2dt} = \frac{k_B T}{\gamma} \tag{12}$$

is the diffusion coefficient. Equation (12) is known as the Einstein relation and is the simplest example of fluctuation-dissipation theorem (FDT). It also provides a useful metric for quantifying the rheological state of a system. By inserting the Stokes expresison for the drag γ we obtain $D = \frac{k_B T}{6\pi\eta R}$ which is known as the Stkes-Einstein relation.

Exercise 1: Green-Kubo formula
Show that the diffusion coefficient can also be written as

$$D = \frac{1}{d}\int_0^\infty dt \langle \mathbf{v}(t)\cdot\mathbf{v}(0)\rangle \ . \tag{13}$$

This is the simplest example of a Green-Kubo formula that expresses a transport coefficient in term of an equilibrium time correlation function.

Note that if we consider from the outset the overdamped limit where $t \gg \tau$, we can neglect inertia in Eq. (5), which reduces to

$$\gamma \frac{d\mathbf{r}}{dt} = \mathbf{f}(t) \ . \tag{14}$$

In this limit the MSD is always diffusive, with

$$\langle [\Delta \mathbf{r}]^2 \rangle = 2dDt \ . \tag{15}$$

Finally, an equivalent description of Brownian motion (or in general stochastic dynamics) is in terms of the probability distribution $P(\mathbf{r}, \mathbf{v}, t)$ of finding the particle in a neighborhood $(d\mathbf{r}, d\mathbf{v})$ of $(\mathbf{r}, \mathbf{v})$ at time t. One can show that the probability distribution of a particle with dynamics described by Eq. (5) is described by a Fokker-Planck equation [32]. Here we are mainly interested in situation where the velocity relaxes very quickly and the dynamics is overdamped. For this reason we will simply consider the distribution $P(\mathbf{r}, t)$ of particles' positions. For concreteness, it is, however useful to consider the case of an overdamped particle subject to a force $\mathbf{F}_e = -\boldsymbol{\nabla} V_e$. The Langeving equation is then given by

$$\gamma \frac{d\mathbf{r}}{dt} = \mathbf{F}_e + \mathbf{f}(t) \ . \tag{16}$$

One can then show that the probability distribution of positions satisfies the following Fokker-Planck equation (usually referred to as Smoluchowski equation in the overdamped limit)

$$\partial_t P(\mathbf{r}, t) = -\frac{1}{\gamma}\boldsymbol{\nabla}\cdot(\mathbf{F}_e P) + D\nabla^2 P \ . \tag{17}$$

B. A single Active Brownian Particle

A minimal models of an active or self-propelled particle is obtained by adding to the particle's dynamics a sustained energy source that embodies the microscopic conversion of energy stored in

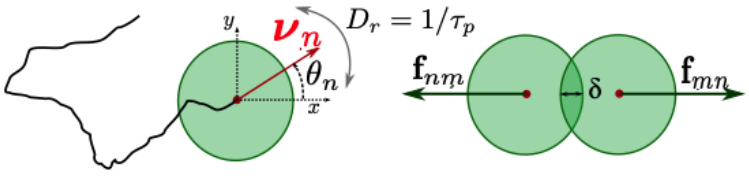

Figure 2. Sketch of an Active Brownian Particle (left) and two particles repelled by soft forces upon overlapping a distance δ.

the environment into directed motion. The resulting propulsion force is subject to fluctuations which are generally not thermal in origin. For simplicity, we neglect inertial effects and restrict ourselves to particles in $2D$. An ABP is then described by the position $\mathbf{r}$ of its center of mass and a unit vector $\boldsymbol{\nu} = (\cos\theta, \sin\theta)$ that denotes the direction of self-propulsion. The translational dynamics is governed by the balance of propulsion, possibly an external potential U, and noise, and is described by the Langevin equation given by

$$\gamma \dot{\mathbf{r}} = f_0 \boldsymbol{\nu} - \boldsymbol{\nabla} U + (2D)^{1/2} \boldsymbol{\eta}(t) \; , \tag{18}$$

where f_0 denotes the propulsive force and $v_0 = f_0/\gamma$ is the propulsion speed, assumed constant. Here $D = k_B T/\gamma$ is the thermal translational diffusion coefficient introduced earlier. Since the variance of thermal noise has been scaled out, the stochastic force $\boldsymbol{\eta}(t)$ is Gaussian distributed with zero mean and unit variance, $\langle \boldsymbol{\eta}(t) \rangle = 0$ and $\langle \eta_i(t) \eta_j(t') \rangle = \delta_{ij} \delta(t - t')$. The direction of the propulsive force changes stochastically according to

$$\dot{\theta} = \sqrt{2 D_R} \; \eta_R(t) \tag{19}$$

where D_R is a rotational diffusion coefficient and $\eta_R(t)$ a Gaussian random force with zero mean and unit variance.

This model captures the directionality of the self-propulsion, namely the ability of the orientation to stay constant during a typical persistence time $\tau_p = D_R^{-1}$ and corresponds to an exponential decay in time of the correlations of the polarity $\boldsymbol{\nu}$,

$$\Big\langle \nu_i(t) \nu_j(0) \Big\rangle = \delta_{ij} \frac{v_0^2}{d} e^{-|t|/\tau} \; . \tag{20}$$

In other words, an ABP can also be thought of as a Brownian particle with colored noise, in addition to δ-correlated thermal noise. Of course colored noise alone would not break detailed balance as the fluctuation-dissipation theorem (FDT) would still hold if the friction were chose to be nonlocal in time. What breaks detailed balance and FDT in this minimal model is the fact that the friction is constant, while the effective noise is correlated in time.

The MSD of a single ABP is given by

$$\Big\langle \Delta \mathbf{r}^2(t) \Big\langle \; = 2d \left(D + D_{\rm sp} \right) |t| + 2 (v_0 \tau)^2 \left(e^{-|t|/\tau} - 1 \right) = \begin{cases} 2dD|t| + v_0^2 t^2 & \text{for } t \ll \tau_p, \\ \\ 2d \left(D_{\rm t} + D_{\rm sp} \right) |t| & \text{for } t \gg \tau_p. \end{cases} \tag{21}$$

with $D_{sp} = v_0^2\tau_p/d$. For a micron-size colloid suspended in water at ambient temperature, the translational diffusion coefficient is of the order of $D_{\simeq}0.1\,\mu\mathrm{m}^2/\mathrm{s}^{-1}$, whereas the active diffusion coefficient of self-phoretic colloids is of the order of $D_{\mathrm{sp}} \simeq 10^2\,\mu\mathrm{m}^2/\mathrm{s}^{-1}$. For this reason in the following we will neglect thermal translational diffusion.

The ABP exhibits ballistic dynamics for $t \ll \tau_p$ and diffusive dynamics for $t \gg \tau_p$. Therefore, the dynamics of an isolated self-propelled particle at times and distances larger than, respectively, the persistence time τ_p and the persistence length $\ell_p = v_0\tau_p$ can not be distinguished from a "hot" Brownian Particle at temperature $T_{eff} = \gamma D_{\mathrm{sp}})$.

ABPs were introduced to mimick the dynamics of self-phoretic colloids with asymmetric chemical and/or physical properties [33, 34]. Other models of self-propulsion have been considered that differ by the assumptions made on the higher order cumulants of the noise statistics. Here we just briefly describe two other models. The run-and-tumble motion is inspired by the dynamics of bacteria [35, 36]. It alternates between an active state when the particles moves at constant speed v_0 in a given direction ("run"), and a passive state when the center of mass of the particle stays constant while reorienting its direction ("tumble"). In practice, the change of direction is taken as instantaneous and completely isotropic, occurring with a given rate α, so that typical trajectories are made of straight lines with random length of typical size v_0/α.

The dynamics of AOUPs was originally proposed as an approximated treatment of ABPs [37, 38]. It consists in neglecting the non-Gaussian nature of the self-propulsion statistics, which amounts to allowing the amplitude of self-propulsion to fluctuate. In practice, such an approximation captures the emergent behavior of ABPs with a better accuracy in three dimensions than two. The self-propulsion dynamics can be described as an Ornstein-Uhlenbeck process

$$\tau_p\dot{\boldsymbol{\nu}} = -\boldsymbol{\nu} + (2D_{\mathrm{sp}})^{1/2}\boldsymbol{\chi}, \tag{22}$$

where $\boldsymbol{\chi}$ is a Gaussian noise with correlations $\langle\chi_\alpha(t)\chi_\beta(0)\rangle = \delta_{\alpha\beta}\delta(t)$ completely uncorrelated with $\boldsymbol{\eta}$. Comparing this to the dynamics of an underdamped passive Brownian particle, we see that the effect of the noise persistence amounts to introducing (i) an effective inertia controlled by the persistence time τ_p and (ii) a velocity-dependent mobility. Moreover, in the limit of vanishing persistence at fixed D_{sp} the original dynamics given in Eq. (18) reduces to the one of an overdamped passive Brownian particle at a temperature $\gamma(D + D_{\mathrm{sp}})$. Therefore, the persistence can be regarded as the only parameter monitoring the nonequilibrium properties of an AOUP [39].

The MSD has the same form for the three models of self-propulsion presented above, since it only depends on the two-point correlations of the fluctuations.

Exercise 2: MSD of a single Active Brownian Particle.
Consider a single APB with dynamics described by the equations

$$\partial_t\mathbf{r} = v_0\boldsymbol{\nu} + \sqrt{2D}\;\boldsymbol{\eta}\;,$$
$$\partial_t\theta = \sqrt{2D_R}\;\eta_R\;,$$

where $\mathbf{r}$ is the center of mass of the particle. The ABP moves with a speed v_0 along a unit vector $\boldsymbol{\nu} = \cos\theta\hat{\mathbf{x}} + \sin\theta\hat{\mathbf{y}}$ that is pinned to its body axis. The self propulsion is not perfect in that it meanders a bit. This is captured by the θ equation where η_R is a stochastic white noise that causes the direction to fluctuate. $\boldsymbol{\eta}$ is the translational white noise that gives rise to diffusion. The noise has zero mean and correlations

$$\langle\eta_i = (t)\,\eta_j\,(t')\rangle = \delta_{ij}\delta\,(t - t')$$
$$\langle\eta_R\,(t)\,\eta_R\,(t')\rangle = \delta\,(t - t')$$

and all higher cumulants are zero, i.e., the noise is Gaussian. Our goal is to compute the MSD of the partcile, i.e., derive Eq. (21) of the notes.$\langle r_\alpha(t)\, r_\beta(t)\rangle$.

1. Show that

$$\langle \boldsymbol{\nu}(t)\, \boldsymbol{\nu}(t')\rangle = \frac{1}{2}\begin{pmatrix} \cos 2\theta_0 \exp\left(-D_R\left[t+t'+2\min(t,t')\right]\right) & \sin 2\theta_0 \exp\left(-D_R\left[t+t'+2\min(t,t')\right]\right) \\ +\exp\left(-D_R\left[t+t'-2\min(t,t')\right]\right) & -\cos 2\theta_0 \exp\left(-D_R\left[t+t'+2\min(t,t')\right]\right) \\ \sin 2\theta_0 \exp\left(-D_R\left[t+t'+2\min(t,t')\right]\right) & +\exp\left(-D_R\left[t+t'-2\min(t,t')\right]\right) \end{pmatrix}$$

2. Now compute $\langle r_i(t)\, r_j(t)\rangle$ (assume $\mathbf{r}(t=0)=0$). You can average over the initial angle θ_0.
3. Now analyze the form of the mean square displacement at short times i.e., $t << \frac{1}{D_R}$ and at long times, i.e., $t >> \frac{1}{D_R}$.
4. Write a program to evaluate numerically the MSD of a single APB neglecting the translational noise and compare your numerical result to your calculation, as well as to the MSD of a single overdamed Brownian particle.
5. Define an effective temperature T_{eff} for your ABP. Research the literature to find suitable parameters for, say, a typical Janus active colloid and evaluate T_{eff}.

C. Adding Interactions

Interactions are of course essential for self-organization. We can classify the type of interactions that have been considered as follows:

- steric interactions: play a key role in driving MIPS and active jamming, but also nematic order if the particles are rod-like;
- aligning interactions: can be polar or apolar in nature, driving flocking or active nematic states;
- shape-based interactions, as in Vertex and Voronoi models used to describe confluent epithelial tissues, which are topological in nature;
- quorum sensing, where microbes interact by secreting some chemical molecules to which other cells respond, or react to the density of their neighbors.

Here we will focus on the first two.

Once interactions are present, it is of course much harder to construct theories capable of predicting the behavior of the system. Most common tools are:

- numerical simulations, either agent-based or particle models;
- continuum theories.

Here we will focus on continuum theories. So let me tell you a bit more about how these can be constructed.

a. How to construct a continuum theory. Often the complexity of the dynamics, inherent to the large number of degrees of freedom, can be reduced by using a continuum description of the system at large scales in terms of a small number of coarse-grained fields. The resulting description is an effective field theory often referred to as hydrodynamics. The first step in constructing a hydrodynamic theory is identifying the fields. To do this, we rely on the notion of separation of time scales: most fluctuations decay on microscopic, short time scales; some, however, are "slow", in the sense that fluctuations of wavelength $\sim 2\pi/q$ decay at a rate $s(q)$ that vanishes when $q \to 0$. A familiar example is diffusion that describes how a local density inhomogeneity or fluctuation $\delta\rho$ decays to eventually reach a state of homogeneous density. This dynamics is governed by the diffusion equation

$$\partial_t \delta\rho = D\nabla^2 \delta\rho \ , \tag{23}$$

where D is the diffusion coefficient. The $\mathbf{q}-$Fourier amplitude of a density fluctuation then decays as $\delta\rho_{\mathbf{q}}(t) \sim e^{-Dq^2 t}$. The decay rate $s(q) = -Dq^2$ vanishes at large wavelength because density is a conserved field ($\int d\mathbf{r}\rho = N$, with N the number of particles in the system) and fluctuations can only decay through material being rearranged from one location to another.

In general, hydrodynamic fields, defined as those whose relaxation rate vanishes when $q \to 0$, are those associated with (i) conservation laws and (ii)spontaneous broken symmetries. If we wish to describe a phase transition, however (as opposed to just the properties of an ordered state), we often include in continuum models the full order parameter even if its magnitude is not strictly a hydrodynamic mode.

Once the relevant fields are identified, the corresponding continuum theory can then be constructed from four different routes:

1. based on phenomenological arguments, such as the symmetries of the system [23, 40];

2. by introducing constitutive equations between the fluxes and the forces identified from the entropy production rate close to equilibrium [41, 42];

3. via explicit coarse-graining of the microscopic dynamics [43–45]. The latter provides explicit expressions for the kinetic coefficients appearing in the theory, whereas such coefficients are unknown *a priori* from the two other methods. Yet, the coarse-graining procedures generally need to be combined with some approximations (e.g., low density, weak interactions) to arrive at some closed form for the dynamical equations.

4. Recently the combination of (i) high resolution imaging that has made available large amount of detailed data, and (ii) machine learning aproaches and data-driven algorythims has provided a new path for learning continuum models from data [46, 47].

Here I will generally just introduce the continuum models with no derivation, but with some justification.

Finally, we should keep in mind that biological systems may be guided by completely different rules, such as the need to optimize information transmission, evolution and survival of the fittest, the development of structures designed to perform specific functions. The notions of broken symmetries and conservation laws inspired by condensed matter physics are very useful, but we must to keep a fresh and open mind in the search for new principles that may govern biology.

IV. SCALAR ACTIVE MATTER: MOTILITY INDUCED PHASE SEPARATION (MIPS)

The name scalar active matter is used to describe systems of isotropic motile particles with radially symmetric interactions. The simplest case is when the interactions are purely repulsive. Even in this simple case, motility can have profound effects on the collective behavior, driving two nonequilibrium phase transitions:

- MIPS: a type of liquid-gas condensation that occurs in the absence of any attractive interactions [3, 4, 33, 34, 36];
- glassy/jammed states at high density, with dynamical heterogeneities and behavior typical of glassed, observed for instance in confluent biological tissue [48–51].

In this lectures I will focus on MIPS. If you are intersted in active jamming, there are some excellent reviews, such as Refs. [49, 51].

To examine the remarkable behavior of a minimal model with just motility and purely isotropic steric interactions, we consider a collection of N disc-shaped ABPs in two dimensions interacting with pairwise repulsive forces. Interactions, even just steric ones, reveal the nonequilibrium nature of ABPs and how motility alone can engender self-organization not possible in equilibrium.

The microscale dynamics is governed by a set of coupled Langevin equations, given by

$$\dot{\mathbf{r}}_n = v_0 \boldsymbol{\nu}(\theta_n) + \frac{1}{\gamma} \sum_{m \neq n} \mathbf{f}_{nm} \ , \tag{24}$$

$$\dot{\theta}_n = \sqrt{2D_{\mathrm{R}}}\ \eta_n, \tag{25}$$

where η_n are uncorrelated Gaussian noises with zero mean and correlations

$$\big\langle \eta_n(t)\eta_m(0)\big\rangle = \delta_{nm}\delta(t). \tag{26}$$

and we have neglected translational thermal noise. The forces $\boldsymbol{f}_{nm} = -\nabla_n V(\mathbf{r}_m - \mathbf{r}_n)$, with $V(\mathbf{r}_n - \mathbf{r}_m)$ the pair potential, are purely repulsive. The results described below do not qualitatively depend on the specific form chosen for the interaction potential. A common form used in the literature are soft repulsive forces $\boldsymbol{f}_{nm} = f_{nm}\hat{\boldsymbol{r}}_{nm}$, with $\hat{\boldsymbol{r}}_{nm} = (\boldsymbol{r}_n - \boldsymbol{r}_m)/r_{nm}$, $r_{nm} = |\boldsymbol{r}_n - \boldsymbol{r}_m|$, and $f_{nm} = k(a_n + a_m - r_{nm})$ if $r_{nm} < a_n + a_m$ and $f_{nm} = 0$ otherwise. Here a_n is the radius of the n-partcile. For monodisperse systems $a_n = a$ independent of n.

Useful dimensionless parameter to describe N ABPs in a $2D$ area A are the packing fraction $\phi = \sum_n \pi a_n^2/A$ and the rotational Péclet number defined as the ratio of the particle persistence length, $\ell_p = v_0\tau_p$, to its size a as $Pe = \ell_p/a$. Numerical simulations of this model show that repulsive ABPs phase separate into a dilute and a dense phase. This is surprising because in equilibrium phase separation requires attractive interactions. For monodisperse particles the dense phase can be hexatic or even crystalline. For polydisperse particles it is glassy. An example of the phase diagram for monodisperse discs from Ref. [52] is shown in Fig. 3.

The transition occurs because crowding slows down the particles' motility, and particles in turn accumulate where they show down, resulting in a runaway effect that leads to a spinodal instability or "antidiffusion". More precisely one can carry out a perturbative (in the density ρ of ABPs) calculation of the effect of interactions on the propulsive speed and show that, to leading order, $v_0 \to v(\rho) = v_0 + \mu\langle \boldsymbol{\nu}_n \cdot \sum_{m\neq n} \mathbf{f}_{nm}\rangle \simeq v_0(1 - \lambda\rho)$, with $\lambda > 0$. The phase separation can also be understood via a nice kinetic argument due to Redner *et al.* [34] that clearly shows that the persistent

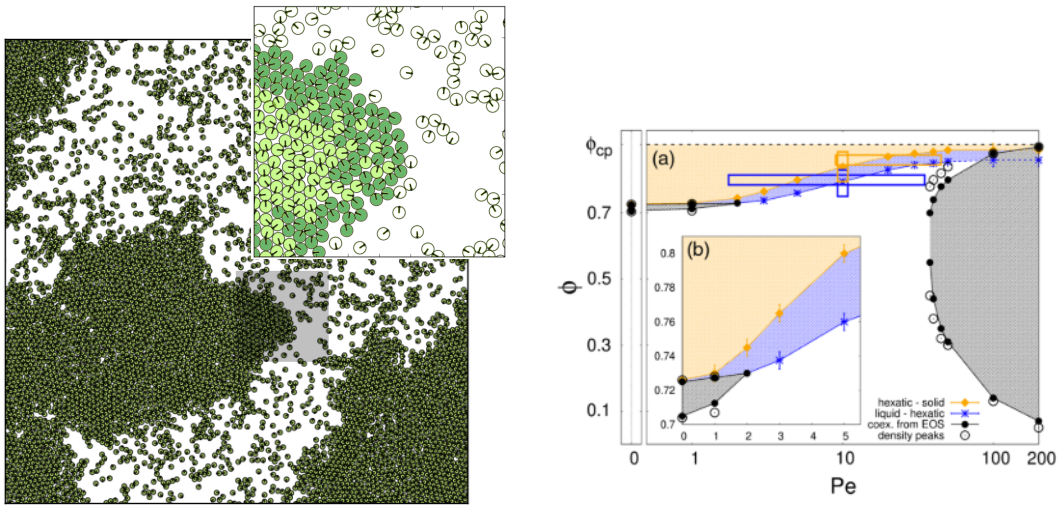

Figure 3. Left: Snapshot from simulations of MIPS. Right: Phase diagram of monodisperse ABPs in the plane of Péclet number Pe and packing fraction ϕ showing the coexistence region (gray), hexatic liquid (purple) and hexatic solid (yellows) regions (from Ref. [52].

dynamics of ABPs breaks detailed balance: the flux of particles into a cluster ($J_{in} \sim \rho_{gas} v_0$) is different from the flux out of the cluster, which is controlled by the rate at which particles turn their nose outward ($J_{out} \sim (\tau_p a)^{-1}$). A simple estimate for phase separation is then given by $J_{in} \sim J_{out}$, which gives $\phi \sim Pe^{-1}$. This also corresponds to the statement that $\tau_p > \tau_{mf}$, with $\tau_{mf} \sim (2av_0\rho)^{-1}$ the mean free time between collisions. In other words, aggregation occurs when colliding particles do not have time to turn their nose away before experiencing more collisions.

The key simplifying feature of this model is that particles do not exert torques on each other nor on the surrounding medium. The angular dynamics of each particle is unaffected by that of the others and by interactions. In fact, as shown at the single particle level, the angular dynamics can be eliminated at the cost of turning the noise in Eq. (24) into colored noise, correlated over a perisistence time $\tau_p = D_R^{-1}$. It is then evident that the model breaks detailed balance in a minimal way because the constant mobility is not balanced by the colored noise.

A. Mean-Field-Theory of MIPS

To construct a simple Mean-Field-Theory of MIPS, we use Eq. (17) to write down the Smoluchowski equation for the probability distribution $\mathcal{P}(\mathbf{r}, \boldsymbol{\nu}, t)$ for an active particle to be at $\mathbf{r}$ with orientation $\boldsymbol{\nu}$ at time t

$$\partial_t \mathcal{P} = -\boldsymbol{\nabla} \cdot (v_0 \boldsymbol{\nu} \mathcal{P}) + D_R \partial_\theta^2 \mathcal{P} \tag{27}$$

The angular moments of $P(\mathbf{r}, \boldsymbol{\nu}, t)$ describe the local properties of ABPs as follows

$$\rho(\mathbf{r}, t) = \int d\boldsymbol{\nu}\ \mathcal{P}(\mathbf{r}, \boldsymbol{\nu}, t) \quad \text{density} \tag{28}$$

$$\mathbf{p}(\mathbf{r}, t) = \int d\boldsymbol{\nu}\ \boldsymbol{\nu}\ \mathcal{P}(\mathbf{r}, \boldsymbol{\nu}, t) \quad \text{polarization density} \tag{29}$$

$$\rho(\mathbf{r}, t) Q_{ij}(\mathbf{r}, t) = \int d\boldsymbol{\nu} \left(\nu_i \nu_j - \frac{1}{d} \delta_{ij} \right) \mathcal{P}(\mathbf{r}, \boldsymbol{\nu}, t) \quad \text{nematic alignment tensor} \tag{30}$$

$$\text{etc.} \tag{31}$$

We can obtain equations for these moments by integrating Eq. (27) over angles, with the result (for $d = 2$)

$$\partial_t \rho = -\boldsymbol{\nabla} \cdot (v_0 \mathbf{p}) \tag{32}$$

$$\partial_t \mathbf{p} = -D_r \mathbf{p} - \frac{1}{2} \boldsymbol{\nabla}(v_0 \rho) - \boldsymbol{\nabla} \cdot v_0 \mathbf{Q} \tag{33}$$

$$\partial_t \mathbf{Q} = -D_r \mathbf{Q} - \boldsymbol{\nabla}(...) \tag{34}$$

Each moment equation couples to higher order moments. To obtain a closed set of equations we neglect $\mathbf{Q}$ and higher moments and assume that for $t \gg D_R^{-1}$ the polarization density can be slaved to the conserved density, i.e., $\mathbf{p} \simeq -\frac{1}{2D_r} \boldsymbol{\nabla}(v_0 \rho)$. Substituting in Eq. (41), we obtain

$$\partial_t \rho = \boldsymbol{\nabla} \cdot \left(\frac{v_0}{2D_R} \boldsymbol{\nabla}(v_0 \rho) \right) = \frac{v_0^2}{2D_R} \nabla^2 \rho \, . \tag{35}$$

Clearly this is just the diffusion equation with diffusion coefficient $D_{sp} = v_0^2/(2D_R)$. It predicts that any fluctuation of the density from its homogeneous equilibrium value $\delta\rho = \rho - \rho_0$ decays in time, with $\delta\rho_{\mathbf{q}}(t) \sim e^{-D_{sp} q^2 t}$ for the decay of the corresponding Fourier amplitude.

As we argued earlier, interactions renormalize v_0 to a $v(\rho) < v_0$. Our MFT is obtained by replacing v_0 in Eq. (35) with $v(\rho)$, with the result

$$\partial_t \rho = -\boldsymbol{\nabla} \cdot \frac{v(\rho)}{2D_R} \boldsymbol{\nabla} \rho v(\rho) - \boldsymbol{\nabla} \cdot [-D(\rho) \boldsymbol{\nabla} \rho + \rho \mathbf{V}(\rho)] \tag{36}$$

where

$$D(\rho) = \frac{(v(\rho))^2}{2D_r} \, ,$$

$$\mathbf{V}(\rho) = -\frac{v(\rho}{2D_R} \boldsymbol{\nabla} v(\rho) \, . \tag{37}$$

Equation (36) is an advection diffusion-equation It can also be written as an effective diffusion equation as

$$\partial_t \rho = \boldsymbol{\nabla} \cdot \mathcal{D}(\rho) \boldsymbol{\nabla} \rho \tag{38}$$

where

$$\mathcal{D}(\rho) = \frac{v(\rho)}{2D_R} [v(\rho) + \rho v'(\rho)] \tag{39}$$

and the prime denotes a derivative wrt ρ. If $v(\rho)$ is a sufficiently strongly decreasing function of ρ, then one can have $\mathcal{D}(\rho) < 0$ and density fluctuations will grow in time signaling, as we will see below, spinodal decomposition and phase separation. Explicit perturbative calculations give, to leading order in the density, $v(\rho) = v_0(1 - \tau_c/\tau_{mf}$, where τ_c is the mean duration of a collision and τ_{mf} the mean free time between collisions [3].

Equation(38) can be derived by explicit coarse graining of the microscopic dynamics. Here we will, however, follow a more generic approach based on field theory ideas and will discuss the implications of the equations in that context. Before doing this, it is useful to review the equilibrium description of phase separation in the context of the so-called Cahn-Hilliard equation or Model B.

Exercise 3: Run-and-Tumble in $1D$.
Consider N particles undergoing run-and-tumble dynamics in one dimensions. These particles tumble at a constant rate α, but their run speed $v(x)$ is spatially varying. Such a situation can be achieved experimentally using, for instance, photokinetic *E.coli* [see G. Frangipane *et al.*, Dynamic density shaping of photokinetic *E. coli*, eLife **7**:e36608 (2018)]. Denote by $R(x,t)$ and $L(x,t)$ the density of right-moving and left-moving particles at time t.

1. Write Smoluchowski equations for the time evolution of R and L.
2. Reformulate the dynamics in terms of the total particle density $\rho = R + L$ and their polarization $p = R - L$.
3. Show that the dynamics can be recast in the mean-field form given in Eqs. (38-37) and identify the expression for $\mathcal{D}$. Clearly state the approximations you need to make to obtain this form and discuss whether you think they may apply to the experiments of Frangipane *et al.*.
4. Find the steady state solution $\rho_{ss}(x)$ of the equation you obtained in item 3 and contrast it to the steady state solution in the case where $v = v_0$.

Problem 3 highlights the difference betweew diffusion and the spontanoeus aggregation that drives MIPS. In equilibrium density inhomogeneities decay via diffusion and the steady state is homogeneous, with $\rho =$ constant. The persistent dynamics of ABPs, in contract, traps particles when their nose points towards high density regions and builds up density inhomogeneities.

The statistical physics of repulsive ABPs has been studied extensively, with the goal of constructing an effective thermodynamics for this system, including defining the pressure of an active gas, an effective surface tension, effective chemical potential, etc. [53].

MIPS has been seen in countless numerical simulations, but has it been seen in experiments? Experimental active systems, living and not, ubiquitously show aggregation in clusters and at surfaces. But are these really examples of MIPS? In general the interpretation of experiments in active colloids is complicated by a variety of phoretic effects, as well as hydrodynamic interactions. Experiments in bacteria are also complicated by hydrodynamic interactions, as well as chemotaxis, quorum sensing and more. The condensation of protein in membrane-free organelles inside living cells and their nucleus is presumably mediated by a variety of chemical reactions. In all these cases one observes arrested (as opposed to bulk) phase separation with the formation of dynamical clusters of well defined mean size. Nonetheless ABPs and their cousin models have allowed us to make great strides in the undertsanding the statitical physics of collection of particles whose dynamics breaks TRS. In fact ABPs have sometimes been referred to as "the Ising model" of active matter.

There are various mechanisms that can arrest phase separation, resulting in the selection of patterns or finite-size clusters. A generic one which is important in biological settings is the breaking of number conservation, as arising from cell division and death. This is achieved for instance by adding a logistic growth term to our MFT of MIPS to obtain dynamics described by the equation

$$\partial_t \rho = \boldsymbol{\nabla} \cdot [\mathcal{D}(\rho) \boldsymbol{\nabla} \rho] + \alpha \rho \left(1 - \frac{\rho}{\rho_0}\right) - \kappa \nabla^4 \rho \,, \tag{40}$$

where ρ_0 is the fixed uniform density of the model and the term proportional to interfacial tension κ is added to ensure stability at short scales. This model, studied for instance in Ref. [54], yields regular lattices of high density spots and concentric high density rings in $2D$, and captures some of the patterns observed in certain bacteria and usually explained by invoking chemotaxis. Pattern formation arises because reproduction and stabilizing surface tension compete with the destabilizing negative diffusivity from crowding, selecting a length scale $\sim \sqrt{|\mathcal{D}(\rho_0)|/\alpha}$.

B. Mapping MIPS onto Cahn-Hilliard-type theory: Model B^+

The phase separation of two immiscible fluids is a common phenomenon in everyday life (just think of oil and vinegar) used for the engineering of a variety of soft material and with important implications in biology. Generally a binary fluid consists of two fluid of A and B molecules that can exist in a well mixed homogeneous state at high temperature and in a demixed state of coexisting A-rich and B-rich phases separated by a fluid-fluid interface at low temperature. In equilibrium the demixing requires interspecies attractive interactions. A related phenomenon is gas-liquid condensation, where condensation again requires attractive interactions.

1. Cahn-Hilliard theory of Phase Separation - a brief review

Phase separation and its kinetics in equilibrium are well described by what are known as Model B and the Cahn-Hilliard equation. There are excellent reviews of this (e.g., Ref. [55]) and I will not spend a lot of time on it, but it is useful to review a few basic notions.

First of all let us remind ourselves of the continuum or field-theoretic model for passive colloidal particles diffusing, for instance, near a substrate, so that momentum is not conserved. The order parameter is the particle density ρ, which is conserved and satisfies the equation

$$\partial_t \rho = -\boldsymbol{\nabla} \cdot \mathbf{J} \tag{41}$$

with

$$\mathbf{J} = -M(\rho) \boldsymbol{\nabla} \mu + \mathbf{J}^N \,, \tag{42}$$

where $M(\rho)$ is a mobility, $\mathbf{J}^N$ is noise and $\mu = \frac{\delta F}{\delta \rho}$ is the chemical potential. The free energy F consists of an ideal gas contribution and a contribution coming from interactions

$$F[\rho] = k_B T \int_{\mathbf{r}} \{\rho[\ln \rho - 1] + f_{int}(\rho)\} \,. \tag{43}$$

The interaction part is at least quadratic in the density and nonlocal. The noise takes the form

$$\begin{aligned}\mathbf{J}^N &= \sqrt{2\rho D(\rho)}\boldsymbol{\eta} \\ \langle \eta_i(\mathbf{r},t)\eta_j(\mathbf{r}',t')\rangle &= \delta_{ij}\delta(t-t')\delta(\mathbf{r}-\mathbf{r}')\end{aligned} \tag{44}$$

In a system in equilibrium where FDT holds, $D(\rho) = k_B T M(\rho)$ and the (noise-averaged) probability distribution $P(\mathbf{r},t)$ of finding the particle at $\mathbf{r}$ at time t is simply the Boltzmann distribution $P_{eq}[\rho] \sim e^{-F[\rho]/k_B T}$, with $F[\rho]$ the coarse grained free energy (at the microscopic level this is of course replaced by the Hamiltonian of the system).

By expanding the free energy in powers of gradients around a reference density ρ_0 and letting $\phi = \rho - \rho_0$ we obtain the familiar ϕ^4 free energy, given by

$$F[\phi] = \int d\mathbf{r} \left[f_0(\phi) + \kappa(\nabla\phi)^2 \right] \ , \tag{45}$$

with

$$f_0(\phi) = \frac{a}{2}\phi^2 + \frac{b}{4}\phi^4 \ , \tag{46}$$

where $b > 0$ and a can change sign as a function of the parameter (say, temperature) that tunes the transition. This Landau free energy can describe gas-liquid condensation (in which case ϕ is the difference between the densities of the dense and dilute phases) or the demixing of a mixture of two immiscible fluids, whereϕ describes the local composition of the binary fluid mixture (hence proportional to the difference between concentration of A and of B molecules [1]).

The homogeneous free energy is $F_0 = V f_0(\overline{\phi})$, with V the volume of the system and we have set $\phi(\mathbf{r}) = \overline{\phi}$ - the homogeneous value. For $a > 0$, f_0 has a single stable minimum at $\overline{\phi} = 0$. For $a < 0$, f_0 has negative curvature for $-\phi_s \le \overline{\phi} \le \phi_s$, where $\phi_s = \sqrt{-a/3b}$ is the spinodal boundary (see Fig. 4). In this region the system is locally unstable. f_0 has two minima at $\overline{\phi} = \pm\phi_b$, with $\phi_b = \sqrt{-a/b}$. For $\overline{\phi}$ the free energy is minimized by a demixed state, with two coexisting states of concentrations $\pm\phi_b$. In other words, at $a = 0$ there is a transition from a homogeneous or well mixed state to a demixed or phase separated one.

Since both ϕ and the volume V are conserved, in the region between the binodals the system splits into two phases of concentration $\pm\phi_b$ and volumes$V_{1,2}$. The partial volumes are determined by the conditions [2]

$$\begin{aligned} V &= V_1 + V_2 \\ V\overline{\phi} &= (V_1 - V_2)\phi_b \end{aligned} \tag{47}$$

The coexisting phase are separated by an interface. The profile of the interface is easily obtained analytically by solving

$$\frac{\delta F}{\delta \phi} = a\phi + b\phi^3 - \kappa\nabla^2\phi = 0 \tag{48}$$

---

[1] Here we consider the simplest case of a symmetric mixture where AA and BB interactions are the same.

[2] In this symmetric case, the free energy at coexistence is determined by the horizontal line connecting $\overset{(}{\pm}\phi_b)$. In a more general case of an asymmetric mixture where we may have linear or cubic terms in $f_0(\overline{\phi})$, this horizontal line would be replaced by a 'common tangent construction' (CTC): a tilted line tangent to $f(\overline{\phi})$ at the coexhisting densities $\phi_{1,2}$. The CTC correpsonds to equality of chemical potential and pressure. in the two coexisting phases.

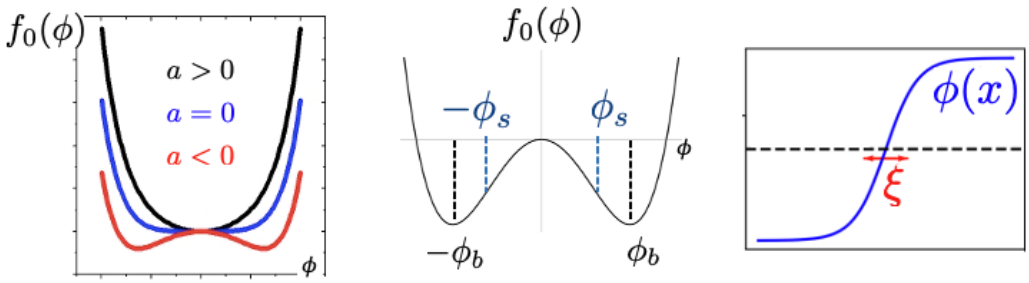

Figure 4. Left: the homogeneous free energy density f_0 is shown as a function of ϕ ($\overline{\phi}$) above ($a > 0$), at ($a = 0$) and below ($a < 0$) the transition. Center: The region $\phi_s \leq |\phi| \leq \phi_b$ is known as the binodal. In this region the homogeneous state is globally unstable, but locally stable, in the sense that a critical size fluctuation (critical nucleus) is required to initiate phase separation. The kinetics in the region proceed via nucleation and one must include noise for a description of the corresponding activated dynamics. The region $|\phi| < \phi_s$ is known as the spinodal region and is locally, as well as globally, unstable, i.e., any infinitesimal perturbation grows and destabilizes the homogeneous state. To describe the dynamics in this region we can neglect noise (but of course one must include some noise in the initial condition when simulating the dynamics). Right: the steady state profile of the interface.

with boundary conditions $\phi(\pm\infty) = \pm\phi_b$, with the result

$$\phi(x) = \phi_b \tanh\left(\frac{x}{\xi}\right) , \tag{49}$$

where we have chosen the midpoint of the interface at $x = 0$. The energy scale κ is a stiffness and controls the surface tension $\sigma = (-8\kappa a^3/9b^2)^{1/2}$ and the thickness $\xi = (-\kappa/2a)^{1/2}$ of the interface.

Note that Eq.(48) sets the exchange chemical potential

$$\mu_{eq} = \frac{\delta F}{\delta \phi} = a\phi + b\phi^3 - \kappa\nabla^2\phi \tag{50}$$

equal to zero. The exchange chemical potential is the difference in the chemical potentials of the two phases.

Exercise 4:
Find the solution of Eq. (48) with the given boundary conditions.

The coarsening dynamics is described by an equation for the conserved field ϕ known as Model B or Cahn-Hilliard equation, given by

$$\partial_t \phi = -\boldsymbol{\nabla} \cdot \mathbf{J}_\phi , \tag{51}$$

$$\mathbf{J}_\phi = -M\boldsymbol{\nabla}\mu_{eq} , \tag{52}$$

where M is the mobility. This is in general a nonlinear function of ϕ but here for simplicity it will be assumed to be constant, with $M = 1$. Explicitely, the Cahn-Hilliard equation is then given by

$$\partial_t \phi = \nabla^2 \left(a\phi + \phi^3 - \kappa\nabla^2\phi\right) \tag{53}$$

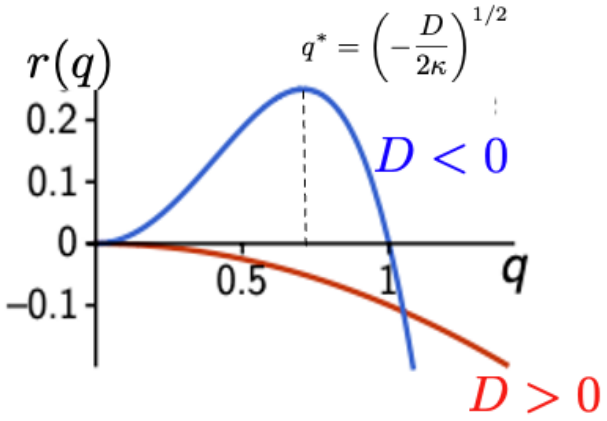

Figure 5. The dispersion relation obatined by lienarized the Cahn-Hilliard equation about a homogeneous state. For $D > 0$ the homogeneous state is stable and fluctuations decay diffusively (red curve). For $D < 0$ the homogeneous state is unstable and fluctuations grow exponentially in a band of wavnumber. The dispersion relation has the characteristic spinodal shape. The wavenumber q^* describes the fastest growing modes.

where without loss of generality I have scaled ϕ to set the coefficient of the ϕ^3 term to unity. To examine the coarsening in the spinodal region, we linearize Eq. (53) about the homogeneous value $\overline{\phi}$ and examine the dynamics of the Fourier amplitudes of the fluctuations $\delta\phi = \phi - \overline{\phi} = \sum_{\mathbf{q}} \delta\phi_{\mathbf{q}}(t) e^{i\mathbf{q}\cdot\mathbf{r}}$, given by

$$\partial_t \delta\phi_{\mathbf{q}} = -q^2 \left(D + \kappa q^2\right) \delta\phi_{\mathbf{q}} \,, \tag{54}$$

where $D = a + 3\phi_0^2$. Fluctuations decay/grow at the rate $r(q)$ according to $\delta\phi_{\mathbf{q}}(t) \sim e^{r(q)t}$. The dispersion relation $r(q)$ is shown in Fig. 5. For $D > 0$, $r(q) < 0$ and fluctuations decay diffusively. For $D < 0$, there is a band of wavenumbers where $r(q) > 0$ and fluctuations grow exponentially. Eventually nonlinearities kick in and stabilize a sharp interface. The system shows a bicontinuos structure and coarsens all the way to bulk phase separation. Late stage coarsening is driven by diffusive fluxes through a process called Ostwald ripening where small droplets shrink and large droplets grow. The scale $L(t)$ of the pattern is set by the wavenumber of the most unstable mode $L(t) \sim 1/q^*$. This grows in time with a characteristic exponent $L(t) \sim t^{1/3}$ and the pattern coarsens all the way to the system size. The 1/3 growth law is easily understood by assuming that growth is controlled by a single length scale L moving at velocity v so that $\dot{L} \sim v$. If the dynamics of the system is dominated by diffusive currents, we estimate $v \sim \nabla\mu_{eq} \sim M\sigma/L^2$, where σ is the interfacial tension and I have restored the mobility M for clarity. Then $\dot{L} \sim M\sigma/L^2$, which gives $L(t) \sim t^{1/3}$.

In equilibrium the change of sign of a is controlled by the interplay of interaction energy versus entropy of mixing, the ϕ^4 term saturates the pattern amplitude, and the κ term cuts off the instability at short scales.

2. A field theory for MIPS

One can construct a field theory of MIPS by mapping the dynamics onto a Cahn-Hilliard-type model [56, 57]. In this mapping the scalar field ϕ is proportional to the difference between the densities of the dense and dilute phases. The MF model of MIPS introduced earlier gives a coventional CH model, where the change of sign of a is controlled by the slowing down of motile particles upon crowding. This is not entirely suprising becasue it has been shown that the effect of motility suppression due to crowding can be mapped onto an effective attractive interaction. The lack of detailed balance in collections of ABPs, however, allows for new terms that are forbidden in equilibrium. The current takes the form [57, 58]

$$\mathbf{J} = -\boldsymbol{\nabla}\mu_{eq} - \lambda\boldsymbol{\nabla}(\boldsymbol{\nabla}\phi)^2 + \zeta(\nabla^2\phi)\boldsymbol{\nabla}\phi \tag{55}$$

When combined with the continuity equation for the ϕ field, Eq. (55) gives what is known as Model B^+. The first term on the right hand side is simply the gradient of the chemical potential obtained as a gradient of the free energy. This term alone preserves TRS and provides the MF description of MIPS given in the previous section. When only this term is retained, one finds that ABPs always coarsen to complete (bulk) phase separation. The other two terms, proportional to λ and ζ, break TRS and cannot be written as derivatives of a free energy. Both these TRS-breaking terms have little effect on the spinodal instability as they do not contribute to linear order. Additionally, the λ term has only a quantitative effect on the phase diagram by shifting the spinodal line to the right or left depending on the sign of λ. The ζ term, however, has qualitative new effects as it can arrest the coarsening via a process dubbed reverse Ostwald ripening, resulting in microphase separation [58]. For more details on these field theories I refer you to the work by the group of Mike Cates and to a review, Ref. [57]. The precise microscopic origin of this terms remains an open question.

C. Nonreciprocal Phase Separation

Multispecies systems with effective cross-interactions that are non-reciprocal, that is evade Newton's third law of action-reaction, have received a lot of interest in recent years [16, 59, 60]. At the microscale, nonreciprocity is intrinsically rooted in the breaking of detailed balance. At a mesoscopic scale, it manifests itself in effective dynamical cross couplings that correspond to non-conservative forces and cannot be obtained as derivatives of a Hamiltonian or free energy. Such non-reciprocity is ubiquitous in active and nonequilibrium systems [61]. It occurs, for instance, in predator-prey systems [62], active solids with odd elasticity [63], protein-based pattern formation [64], mixtures of active and passive particles [59, 65], directional interface growth [66], and non-Hermitian quantum systems [67]. Such systems can spontaneously organize in dynamical steady states with nontrivial temporal order, such as traveling and oscillating states.

In the context of our discussion, a minimal system that highlights the consequences of NR interactions is a mixture of active and passive Brownian particles. The active particles can undergo MIPS, and in MF their dynamics can be described by a Cahn-Hilliard-type equation. The passive particles are simply diffusive. The two are additionally coupled by cross-diffusivities. If we denote by ρ_A and ρ_P the conserved densities of active and passive particles, their coupled dynamics can be described by the following set of equations [68]

$$\partial_t\rho_A(x,t) = \nabla^2(D_{AA}\rho_A + \rho_A^3 - \kappa\nabla^2\rho_A + D_{AP}\rho_P)\,, \tag{56}$$

$$\partial_t\rho_P(x,t) = \nabla^2(D_{PP}\rho_P + D_{PA}\rho_A)\,. \tag{57}$$

These equations can be derived by coarse-graining the microscopic dynamics [59, 65]. In general, all the diffusivities D_{ab} are found to be nonlinear functions of the densities. For simplicity, here we will assume them constant. Since these fields are conserved, the dynamics of fluctuations is controlled by soft or hydrodynamic modes, defined as those where a fluctuation of wavenumber q decays (or grows) at a rate $\sigma(q)$, with $\lim_{q\to 0} \mathrm{Re}[\sigma(q)] = 0$. In the absence of cross couplings, fluctuations in ρ_P decay diffusively, while D_{AA} can become negative in a range of densities and Péclet numbers as the persistent dynamics of ABPs drives MIPS. Therefore fluctuations in ρ_A exhibit the characteristic dispersion relation of a spinodal instability, with largest growth at a characteristic length scale controlled by $|D_{AA}|$ and κ. Cross-diffusion couples the two hydrodynamic modes, but the dispersion relation branches do not cross for cross diffusivities that are equal or obey Onsager's rules (Fig. 6(a)). On the other hand, active particles are slowed down by both other active particles, as well as by passive particles. For this reason, the cross diffusivity D_{AP} can also be negative in a range of densities. Passive Brownian particles, in contrast, undergo conventional diffusions, hence D_{PP}, $D_{PA} > 0$. There is therefore a regime of parameters where the two density fields are coupled not just non-reciprocally, but antagonistically, i.e., $D_{AP} < 0$, $D_{PA} > 0$. One can show that nonreciprocal cross-diffusivities cause the two modes to cross, where the two eigenvectors align at the crossing point, resulting in the appearance of an imaginary part of the dispersion relation [green dashed lines in Fig. 6(a)]. In other words, nonreciprocal couplings lead to mode coalescence and transform the static phase separated state into traveling [Fig. 6(c)] or oscillating domains [59, 60].

Again here a linear stability analysis of the homogeneous state provides much insight. If we linearize the equations about a global steady state, $(\rho_A, \rho_P) = (\rho_A^0, \rho_P^0)$, for perturbations of the form $e^{iqx+\sigma t}$ we find that the modes governing the time evolution of fluctuations are the eigenvalues of the Jacobian

$$J = q^2 \begin{pmatrix} -D_{AA} - 3(\rho_A^0)^2 - \kappa q^2 & -D_{AP} \\ -D_{PA} & -D_{PP} \end{pmatrix} \tag{58}$$

In the uncoupled case ($D_{AP}D_{PA} = 0$), the dispersion relation has two independent branches given by the diagonal entries in the Jacobian [see Fig. 6(a), left frame]. A band of unstable modes $[0, q_+]$ emerges in the first branch when $D_{AA} < -3(\rho_A^0)^2$, where $q_+^2 = (-D_{AA} - 3(\rho_A^0)^2)/\kappa$. This is the spinodal decomposition instability that drives phase separation. Cross-diffusive couplings cause the branches of the dispersion relation to interact near their intersection point, giving rise to a band of propagating modes ($\mathrm{Im}[\sigma] \neq 0$) in the anti-reciprocal case $D_{AP}D_{PA} < 0$; see Fig. 6(a), right frame. For sufficiently strong anti-reciprocal coupling, the band of propagating modes begins to overlap with the band of unstable modes $[0, q_+]$. For $D_{AP}D_{PA} = -D_{PP}^2$, the marginal mode q_+ touches the band of propagating modes. At this point, the Jacobian has two vanishing eigenvalues and is non-diagonalizable, i.e., its eigenvectors coincide. This marks an "exceptional point" [61, 67].

On the basis of the linear stability analysis one can construct a phase diagram (see Fig. 7) that reproduces well the reuslt of numerical integration of the equations.

Note that the traveling waves break both TRS and parity ($\mathbf{r} \to -\mathbf{r}$). Hence this is referred to as a PT-breaking transition.

There are two new findings here. First, while TW and oacillations are ubiquitous and well understood in nonlinearly dynamical systems with activator/inhibitor couplings through models with with few degrees of freedom (e.g. FitzHugh–Nagumo equations [69, 70]) they are unexpected in purely diffusive systems and generally less explored in spatially extended systems. On the other hand, the appearance of TW may not be so suprising as it is the result of the antagonistic cross-diffusivities: active particles are effectively attracted to passive ones, but passives one are repelled by active ones through steric effects. This leads to a chase-and-run dynamics where the two fields eventually settle into a state where they travel at a relative constant velocity. More suprising,

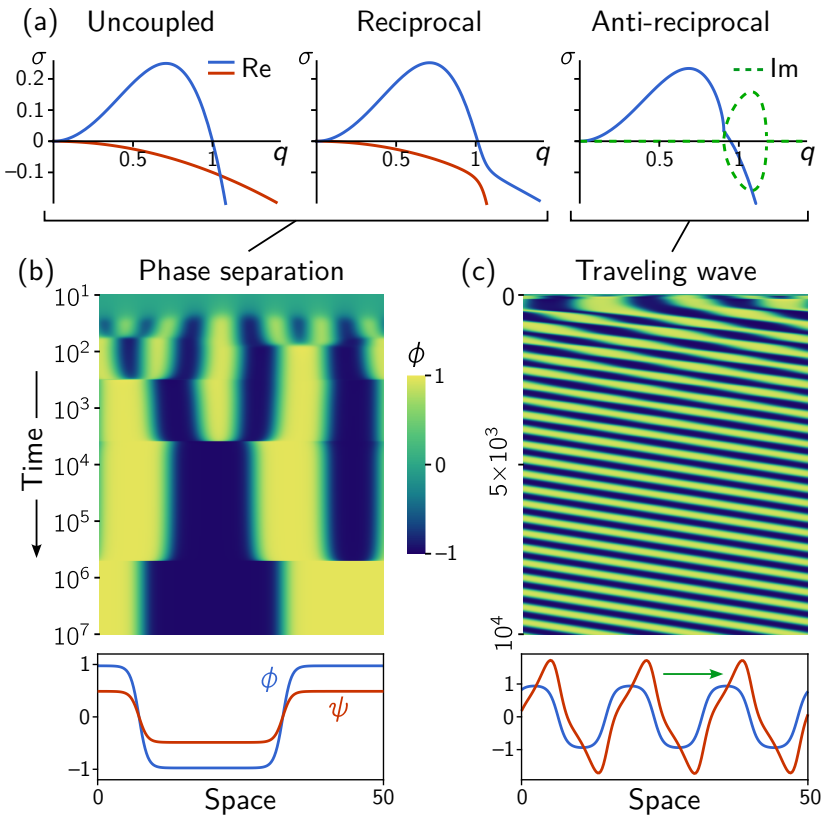

Figure 6. (a) Dispersion relations for the cases $D_{AP} = D_{PA} = 0$ (left), $D_{AP}D_{PA} > 0$ (center) and $D_{AP}D_{PA} < 0$ (right). (b) A kymograph showing the coarsening of the two densities all the way to bulk phase separation for reciprocal couplings. Here $\phi \equiv \rho_A$ and $\psi \equiv \rho_P$. (c) A kymograph showing the arrested coarsening of the two densities and onset of traveling waves for non reciprocal couplings.

however, is that one also gets patterns (not just bulk phase separation) of well-defined wavelength. This is suprising becasue the model itself only contains one length scale (the interface width). The mechanisms for wavelength selection are still under investigation [68]. There are also secondary instabilities, such as traveling undulations that travel along stripes, that are very intriguing.

A similar mechanism is at play in the antagonistic coupling of two groups of flocking agents described for instance by non-reciprocally coupled Toner-Tu equations [61]. In the absence of coupling, each population undergoes a phase transition to a state of finite mean motion that spontaneously breaks polar symmetry [23] - the nonequilibrium analog of a finite magnetization in interacting XY spins. When the two populations A and B are coupled antireciprocally (A wants to align with B, but B wants to antialign with A) the system is dynamically frustrated and organizes into a state of chase-and-run motion, where birds chase each other tails, that breaks chiral symmetry [61]. Both sets of results have opened up a flurry of activity on the role of non-reciprocity in dynamical pattern formation [16] and the search for generic models of nonequilibrium transitions from static to time-ordered states [71].

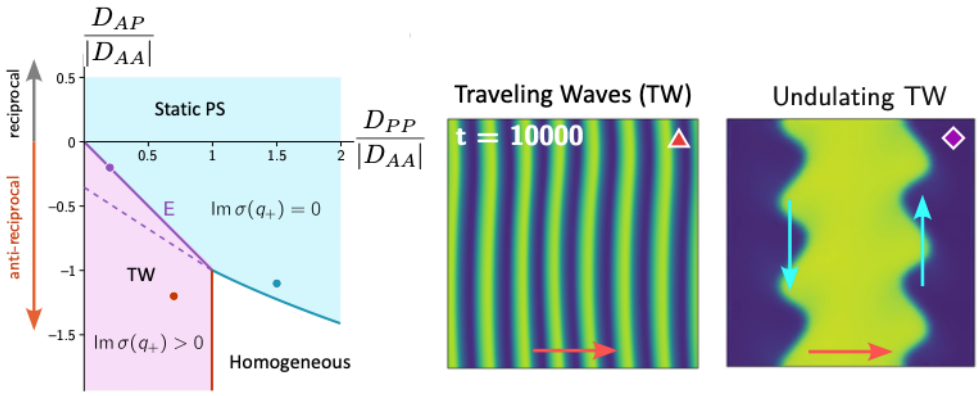

Figure 7. Left: Linear stability diagram in the D_{PP}-D_{AP} parameter plane where we set $D_{AP} = |D_{PA}|$, such that the sign of D_{AP} determines whether the coupling is reciprocal ($D_{AP} > 0$) or anti-reciprocal ($D_{AP} < 0$). Along the purple line (E) an "exceptional point" appears in the dispersion relation, where the band of unstable modes touches the band of propagating modes. When the diffusion of ρ_P is fast (large D_{PP}) pattern formation is suppressed and the homogeneous well mixed state is again stable. Middle: traveling waves (TW) in $2D$. Right: undulating traveling waves in $2D$.

There are two additional important points to be made. First, the structure of the linear fluctuation spectrum seen in the NRCH model (merging of the real part of the two hydrodynamic modes and simultaneous emergence of a finite imaginary part, associated with the non-diagonalizable form of the matrix that governs the linear dynamics of fluctuations and degenerate eigenvectors → exceptional point) is a distinct signature of temporal organization, hence provides a criterion for identifying a new class of dynamical pattern formation (see also [71]). This mechanism is analogue to the one responsible for the onset of chiral states in antagonistic flocking models [61]. There is, however, a difference between the two systems. In NRCH the hydrodynamic nature of the fluctuations guarantees that for strong enough nonreciprocity the merging will occur for all parameter values, hence it is generic. In flocking models the velocity order parameter is not conserved. Instead, the spontaneously broken rotational symmetry of the flocking state is associated with the emergence of a Goldstone mode with relaxation rate that vanishes at long wavelength. The mode coalescence therefore happens *globally* instead of *locally*.

Second, there are a number of experimental systems where TW and oscillations have been observed that can all be recast in the NRCH framework. In addition to the active/passive particles mixture discussed earlier, other examples are mass-conserving reaction-diffusion systems, viscoelastic gels and active interfaces [68].

Exercise 5:
(a) Find eigenvalues and eigenvectors on the matrix given in Eq. (58) and plot the reuslting disperion relations to obtain plots similar to those shown in Fig. 5.
(b) A press release by Ramin Golestanian in Europhysics News hihglights the rapidly growing interest in nonreciprocal interaction in non-equilibrium systems (`https://www.europhysicsnews.org/articles/epn/pdf/2024/03/epn2024553p12.pdf`).
Research the literature to identify an experimental system where traveling and/or oscillating

states are observed and the dynamics can be mapped onto the NRCH model. Address the following questions:

(i) Which are the coupled hydrodynamic fields at play in the system of your choice?

(ii) Why are they "hydrodynamics" (conserved fields, Goldstone modes, other)?

(iii) What are the physical mechanisms that engender effective NR interactions?

(iv) What are the experimental observation?

(v) Do you think the system you have identified is a promising candidate for observing some of the predictions of NRCH models? What would you measure to establish the connection?

V. NEMATIC LIQUID CRYSTALS

Nematic order is seen in many active and biological systems, from chromosome territories to cell monolayers (epithelial cells, stem cells) to entire organisms. There are many reviews with plenty of theoretical and experimental references, such as Refs. [9**? ?** , 10]. The majority of the work so far has focused on active nematic liquid crystals. These are fluids, where the interplay of orientation and active flows drives a rich array of new phenomena, including self-sustained turbulent-like flows. At the end of this set of lectures we will also highlight the role of activity and nematic order in elastic systems, which is relevant to some biological settings, such as the regeneration of *Hydra* [72–74].

Before doing so, we will, however, spend some time introducing material that we will need later in the lectures: how we quantify nematic order, how do we charaterize the excitations that can occur in nematics, both smooth deformations and toplogical defects, how to describe the properties of nematics at the continuum level.

A. Quantifying nematic order

Crystals have both translational (T) and orientational (O) order (long-ranged in $3D$, quasi-long-ranged in $2D$). Liquids have neither. Liquid crystals (LCs) are fluids of macromolecules that can exist in states with O order, but no (or partial) nT order. The simplest example is a nematic LC, a fluid of rod-like molecules that can align their orientation in a spontaneously chosen direction.

Active units are often eleongated and can align due to a variety of interactions, organizing in states with orientational order [3]. While all of you are likely familiar with the vectorial order parameter used to quantify polar order, such as the magnetization of a ferromagnet, some may not not be as familiar with apolar or nematic order. To understand the distinction between the two it is important to keep in mind that

$$\text{direction} \quad \neq \quad \text{orientation}$$

To quantify this distinction, let us consider one of the rod-like particles that compose the system and identify its orientation in space by a unit vector $\hat{\boldsymbol{\nu}}$. We also denote by $\Psi(\hat{\boldsymbol{\nu}})$ the probability density of molecular directions for the tagged rod, with $\int d\hat{\boldsymbol{\nu}}\Psi(\hat{\boldsymbol{\nu}}) = 1$. The explicit form of the probability density will of course depend of other rods and their interactions, but is not needed for the considerations below.

---

[3] Collisions among rod-like particles with steric interactions do of course induce alignment. It has been shown, however, that self-propelled rods with purely steric interactions, which are agnostic to the polarity induced by self-propulsion, order in nematic, not polar states, at large scales [75].

a. Isotropic state. In this case all orientations are equally probable, hence Ψ must be constant, with

$$\Psi_{\rm iso}(\hat{\boldsymbol{\nu}}) = \frac{1}{2^{d-1}\pi} \ , \tag{59}$$

for $d = 2, 3$.

b. Polar/ferromagnetic ordered state. The first moment of Ψ, defined as

$$\mathbf{m} = \int d\hat{\boldsymbol{\nu}} \ \hat{\boldsymbol{\nu}} \Psi(\hat{\boldsymbol{\nu}}) \tag{60}$$

will be nonzero in the ordered state. This quantity vanishes in the isotropic state where Ψ is given by Eq. (59), hence it provides a suitable order parameter for polar order.

c. Apolar/nematic ordered state If the particles are apolar, I can still use $\hat{\boldsymbol{\nu}}$ to identify their orientation, but in this case $\hat{\boldsymbol{\nu}} = -\hat{\boldsymbol{\nu}}$. and Ψ must satisfy $\Psi_N(\hat{\boldsymbol{\nu}}) = \Psi_N(-\hat{\boldsymbol{\nu}})$. The first moment of Ψ_N as defined in Eq. (60) then vanishes and a vector order parameter does not capture nematic order. The first nonzero moment of Ψ_N will be

$$M_{ij} = \int d\hat{\boldsymbol{\nu}} \ \hat{\nu}_i \hat{\nu}_j \Psi_N(\hat{\boldsymbol{\nu}}) \ . \tag{61}$$

In the isotropic state $M_{ij} = \frac{1}{d}\delta_{ij}$. An order parameter that captures nematic order and vanishes in the isotropic state is then

$$Q_{ij} = \int d\hat{\boldsymbol{\nu}} \ \left(\hat{\nu}_i \hat{\nu}_j - \frac{1}{d}\delta_{ij} \right) \Psi(\hat{\boldsymbol{\nu}}) \ . \tag{62}$$

This is known as the de Gennes Q-tensor and provides a suitable order parameter for a uniaxial nematic - the simplest of liquid crystals. A more general many-body definition will be given below.

B. Landau-de Gennes theory of passive nematic liquid crystals

Fluids of elongated macromolecules can be driven to undergo a transition from an isotropic to a nematic state either upon lowering the temperature (thermothropic LCs) or upon increasing the density (lyothropic LCs). The Isotropic-Nematic (IN) transition occurs in systems of purely repulsive hard rods as the result of the interplay of steric effects and entropy, as shown by Onsager in 1949. Essentially, rods gain entropy, hence lower their free energy, by aligning. We can understand this by a simple argument. Entropy can be computed as $S = k_B \ln(\#\text{states})$. For an ideal gas in a volume V, $S_{id} \sim k_B \ln V^N$. If we take into account excluded volume, the entropy is lowered and can be roughly estimated as $S \sim \ln(V - v_{ex})^N$. Clearly S increases as v_{ex} decreases, and aligned rod have a smaller excluded volume that rods at some angle to each other (see Fig. 8). So by aligning, rods increase S and decrease $F = U - TS$.

As suggested by the argument, presented in the previous section the order parameter that captures uniaxial nematic order is a symmetric and traceless tensor, known as the Q-tensor. It can be defined at a microscopic level as the average of the molecular orientations $\hat{\boldsymbol{\nu}}_n$, of the n-th rod as

$$Q_{ij}(\mathbf{r}, t) = \frac{1}{\rho} \langle \sum_n (\hat{\nu}_{ni}\hat{\nu}_{nj} - \frac{1}{d}\delta_{ij}) \delta(\mathbf{r} - \mathbf{r}_n(t)) \rangle \ , \tag{63}$$

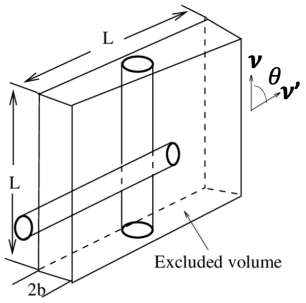

Figure 8. The excluded volume of two rods of diameter b at an angle θ to each other is $2bL\sin\theta$.

where $\rho(\mathbf{r},t)$ is the number density. At the mesoscopic level it can be written as

$$Q_{ij}(\mathbf{r},t) = S(\mathbf{r},t)\left(n_i(\mathbf{r},t)n_j(\mathbf{r},t) - \frac{1}{d}\delta_{ij}\right) , \tag{64}$$

where $S(\mathbf{r},t)$ is a scalar that captures the degree of nematic order and $\mathbf{n}(\mathbf{r},t)$ is a unit vector known as the director field that describes the direction of spontaneously broken symmetry. In $2D$ the director field is $\mathbf{n} = (\cos\theta, \sin\theta)$ and

$$\mathbf{Q} = \frac{S}{2}\begin{pmatrix}\cos 2\theta & \sin 2\theta \\ \sin 2\theta & -\cos 2\theta \cdot\end{pmatrix} \tag{65}$$

Explicit expressions for $\mathbf{Q}$ in $3D$ can be found in textbooks.

The IN transition can be described phenomenologically by the Landau-de Gennes (L-deG) free energy, which is written as an expansion in powers of scalar invariants of the tensor Q_{ij}, as

$$F_{LdG} = \int_{\mathbf{r}}\left[\frac{a(\rho)}{2}|\mathbf{Q}^2| - \frac{w}{3}|\mathbf{Q}|^3 + \frac{b}{4}|\mathbf{Q}^2|^2\right] , \tag{66}$$

where $|\mathbf{A}| = A_{ii}$ denotes the trace of the tensor $\mathbf{A}$ and $a(\rho) = a_0(1-\rho/\rho^*)$, with $w, b > 0$. In $3D$ the LdeG free energy yields a first order transition from an isotropic state with $S = 0$ for $\rho > \rho_{IN}$ to a nematic state for $\rho > \rho_{IN}$. The choice $w = a_0\rho/\rho^*$ and $b = a_0\rho/\rho^*$ gives $\rho_{IN} \simeq 8\rho^*$ and $S = \frac{1}{4} + \frac{3}{4}\sqrt{1 - \frac{8\rho^*}{9\rho}}$. In the following we will focus on $2D$ systems. In this case one can show that $|\mathbf{Q}^3| = 0$ identically and the IN transition is continuous, with $\rho_{IN} = \rho^*$. Then $S = 0$ in the isotropic state for $\rho < \rho_{IN}$ and $S = \sqrt{-2a(\rho)/b}$ in the nematic state for $\rho > \rho_{IN}$.

Gradients of the tensor order parameter field introduce an elastic energy, given by

$$F_e = \int_{\mathbf{r}}\left[\frac{L_1}{2}(\partial_k Q_{ij})(\partial_k Q_{ij}) + \frac{L_2}{2}(\partial_i Q_{ik})(\partial_J Q_{ik}) + \frac{L_3}{2}Q_{ij}(\partial_i Q_{kl})(\partial_j Q_{kl})\right] . \tag{67}$$

Deep in the nematic state, we can assume $S \sim$ const. and neglect fluctuations of the order parameter. The elastic free energy then reduces to the Frank free energy, given by

$$F_K = \frac{1}{2}\int_{\mathbf{r}}\left[K_1(\boldsymbol{\nabla}\cdot\mathbf{n})^2 + K_2(\boldsymbol{\nabla}\times\mathbf{n})^2 + K_3(\mathbf{n}\cdot\boldsymbol{\nabla}\times\mathbf{n})^2\right] . \tag{68}$$

Figure 9. Splay (left), twist (center) and bend (right) deformations of the director field.

The Frank elastic constants K_1, K_2 and K_3 describe, respectively, the energy cost of splay, twist and bend deformations (see Fig. 9). They have dimensions of energy/length in $3D$ (of energy in $2D$) and are related to L_1, L_2 and L_3 as

$$\begin{aligned} L_1 &= \frac{3K_2 - K_1 + K_3}{6S^2} \ , \\ L_2 &= \frac{K_1 - K_2}{S^2} \ , \\ L_2 &= \frac{K_3 - K_1}{S^2} \ . \end{aligned} \tag{69}$$

In $2D$ there are no twist deformations and the Frank Free energy simply reads

$$F_K = \frac{1}{2}\int_{\mathbf{r}} \left[K_1(\boldsymbol{\nabla}\cdot\mathbf{n})^2 + K_3(\mathbf{n}\cdot\boldsymbol{\nabla}\times\mathbf{n})^2\right] \ . \tag{70}$$

In the following we will often use the one elastic constant approximation, setting $K_1 = K_2 = K_3 = K$. The Frank free energy can then be written in a deceiptevely simple form in $2D$, as

$$F_K = \int_{\mathbf{r}} \frac{K}{2}(\boldsymbol{\nabla}\theta)^2 \ . \tag{71}$$

This shows that in equilibrium a $2D$ nematic has the same long distance description as an XY model.

As an aside, it is worthwhile to note that in $2D$, there is no difference between a polar (vectorial) and apolar (nematic) field at the level of the equations themselves, as long as one does not mix spatial and field indices. If such a separation is imposed, the spatial rotations and rotations of the order parameter field decouple and become independent symmetry operations. The difference in the global structure of the order parameter spaces in the two cases manifests itself only through the character of the topological defects. On the other hand, if, as in our case and as inevitable in a liquidm crystal, one does have spatial indices contracted with field ($\mathbf{Q}$ or $\mathbf{n}$) indices, then only the combined simultaneous rotation of both spatial coordinates and the order parameter field together becomes a symmetry operation, in which case the terms permitted in the equations themselves now do depend explicitly on the nature and symmetry of the order parameter field itself [76].

Exercise 6:
Derive the Frank free energy (Eq. (68) from Eq. (67).

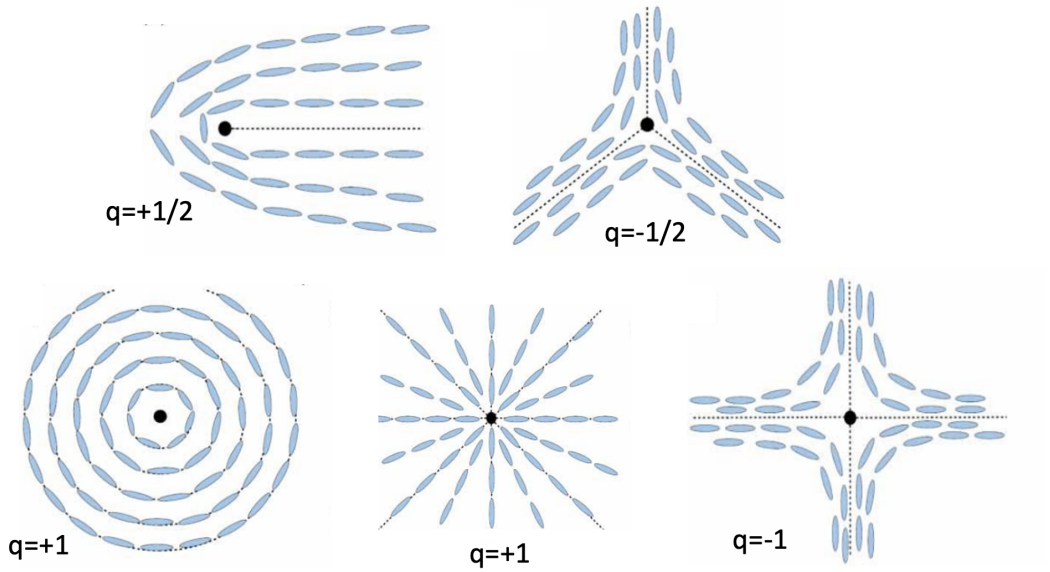

Figure 10. Structure of topological defects that can occur in an uniaxial nematic liquid crystal in $2D$.

C. Topological defects

At any finite temperature, the order of the nematic state is disrupted by excitations. Smooth deformations of the director field are analog to "spin waves" in ferromagnets. They consists of bend and splay deformations in $2D$, and additionally twist deformations in $3D$.

In addition, the order can be interrupted by topological defects, which are singular disruptions of orientational order where the order parameter S vanishes and essentially the director does not know where to point. In passive materials, topological defects are inevitably formed in quenches from the disordered into the ordered state or when order is frustrated by curvature, external fields, or boundary conditions. In active systems defects can be generated spontaneously by activity. Recent work has suggested that biological systems may exploit this connection between structure and dynamics and use defects to localize stresses and perform specific biological functions, such as cell extrusion and death in epithelia and specific morphogenetic processes (the formation of tentacles, mouth or foot) in the development of the freshwater polyp *Hydra* [72, 77–82].

For simplicity we restrict ourselves to $2D$. Defects arise where the director angle $\theta(\mathbf{r})$ is ill-defined and the magnitude S of the order parameter vanishes. In $2D$ defects are point-like excitations (they become lines in $3D$). They are classified by their topological charge or winding number q, defined as

$$q = \frac{1}{2\pi} \oint \boldsymbol{\nabla}\theta \cdot d\mathbf{l} \tag{72}$$

where the integral is taken around a closed loop enclosing the defect. Because of the $\mathbf{n} = -\mathbf{n}$ symmetry, allowed charges are half-integer multiples. The $q = \pm 1/2$ defects, known as disclinations, are energetically favored and dominate the defect population in both thermal and active systems.

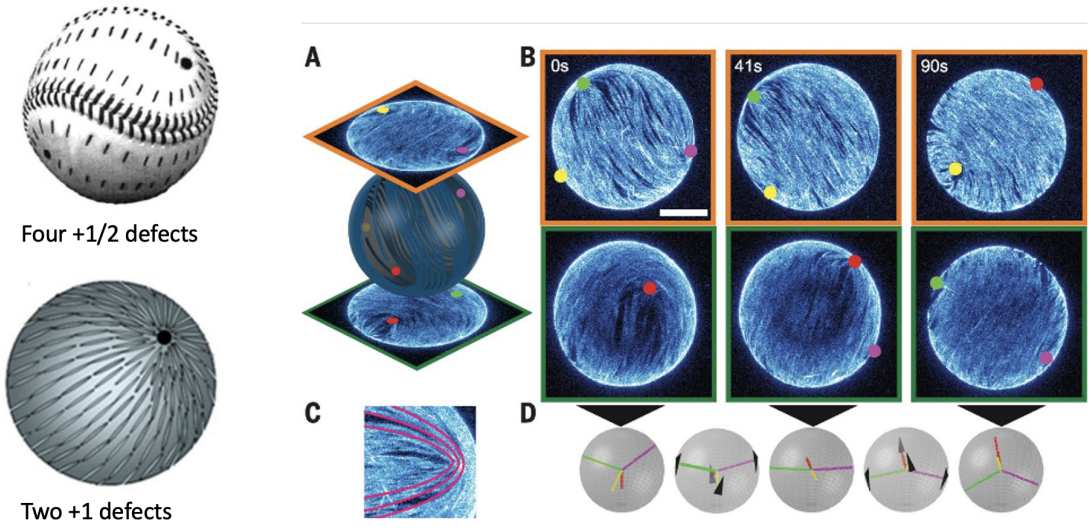

Figure 11. Left: Structure of topological defects on the surface of a sphere decorated with nematic order. In equilibrium the lowest energy configuration is that of four $+1/2$ defects located at the corner of a tetrahedron inscribed in the sphere. Right: When an active microtubule nematic is confined to the surface of a sphere the defects become motile and the four $+1/2$-defect structure exhibits regular oscillations.

They correspond to topological defects in crystalline solids, known as dislocations. Structurally, $+1/2$ defects exhibit a polar, comet-like director configuration, while $-1/2$ defects have a threefold symmetric, trefoil-like structure, as shown in Fig. 10. As we will see below, this distinction has important dynamical consequences in active nematics.

You can easily convince yourself that half-integer defects cannot occur in a polar vector field. In this case the lowest charge defects are ± 1 in this sense, defects are true fingerprints of the broken symmetry. The observation of half-integer topological defects in microtubule-kinesin suspension was key in revealing the nematic symmetry of these systems.

Topological charge is a conserved invariant. The Euler theorem of topology which relates the number of vertices, edges and faces of any tessellation of a two-dimensional manifold tells us that the net topological charge must be zero in the plane, must add up to $+1$ in a disc and to $+2$ on the surface of a sphere. These results will become important when we will discuss the role of topology in the development of *Hydra*.

Topological defects can be described as quasi-particle excitations. Defects distort orientational order and cost elastic energy. They are global excitations, in the sense that the distortion generated by a defect extends to the entire system. In the one-constant approximation, an isolated defect of charge q has a logarithmically divergent energy $E_q = \pi K q^2 \ln(L/a)$, where L is the system size and a is a core cutoff. Hence ± 1 defects are energetically four time as costly as $\pm 1/2$ and in equilibrium spontaneously decay in half-integer defects. Defect interactions are Coulomb-like: pairs of opposite charge attract, while like charges repel, with an interaction energy $E_{12} = -2\pi K q_1 q_2 \ln(r/a)$ for defects of charge q_1 and q_2 separated by a distance r. The mapping of the statistical physics of defects in $2D$ onto that of a $2D$ Coulomb gas underlies the Kosterlitz–Thouless mechanism for the isotropic–nematic transition, in which unbinding of defect pairs destroys quasi-long-range

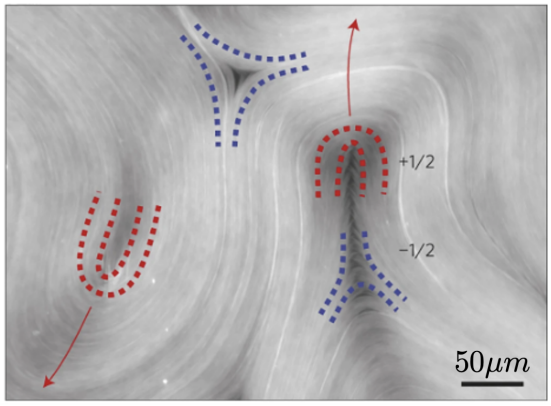

Figure 12. Defects in microtubule-kinesin active nematics, where the +1/2 become motile particles.

orientational order. We refer to standard textbooks for details.

We will see below that in active matter defects acquire a new life and become themselves motile particles, driving the dynamics of the system.

D. Nematohydrodynamics

The dynamical behavior of nematic liquid crystals can be described at the continuum level by coupled equations for the Q-tensor and the flow velocity $\mathbf{v}(\mathbf{r},t)$. In general, a nematic liquid crystals is a suspension of nematogens in a solvent, and its continuum dynamics should be described by a two-fluid model in terms, for instance, of densities and momentum densities for each of the two components. For simplicity we consider here a single fluid model that negelects differences in the flow velocity of nematogens and solvent and describe the system as incompressible fluid with constant density. . The nematohydrodynamic equations then take the form

$$D_t\mathbf{Q} + [\mathbf{\Omega}\cdot\mathbf{Q}]^A = \frac{\lambda}{2}[\boldsymbol{\nabla}\mathbf{v} + (\boldsymbol{\nabla}\mathbf{v})^T] + \frac{1}{\gamma}\mathbf{H}\,, \tag{73}$$

$$\rho D_t\mathbf{v} = -\boldsymbol{\nabla}P + \eta\nabla^2\mathbf{v} + \boldsymbol{\nabla}\cdot\boldsymbol{\sigma}^e\,, \tag{74}$$

and $\boldsymbol{\nabla}\cdot\mathbf{v} = 0$. The order parameter is advected and rotated by flow ($D_t = \partial_t + \mathbf{v}\cdot\boldsymbol{\nabla}$, $\Omega_{ij} = \frac{1}{2}(\partial_i v_j - \partial_j v_i)$, and $([\mathbf{\Omega}\cdot\mathbf{Q}]^A)_{ij} = \Omega_{ik}Q_{kj} - Q_{ik}\Omega_{kj}$) and relaxes at a rate controlled by the molecular field $\mathbf{H} = -[\frac{\delta(F_Q+F_e)}{\delta\mathbf{Q}}]^{ST}$, with γ the rotational viscosity. The flow alignment parameter λ is a material property that describes how the liquid crystal responds to shear flows: the homogeneous solution for the angle θ that the director forms with the direction of flow away from the boundaries is $\cos 2\theta = \frac{1}{\lambda}$ provided $|\lambda| \geq 1$, known as flow aligning. If $|\lambda| < 1$ there is no steady state and the solution is flow tumbling, whereby the director rotates without settling at any particular angle. The parameter λ is determined by microscopic properties of the material, including molecular shape: $\lambda > 0$ for rod-like or prolate particles, and $\lambda < 0$ for disklike or oblate particles. The flow is governed by the Navier-Stokes equation that includes pressure gradients, viscous dissipation with

shear viscosity η, and elastic stresses $\boldsymbol{\sigma}^e$ given by

$$\boldsymbol{\sigma}^e = -\frac{2\lambda}{d}\mathbf{H} - \lambda\left[\mathbf{H}\cdot\mathbf{Q} + \mathbf{Q}\cdot\mathbf{H} - \frac{2}{d}\mathbf{1}|\mathbf{Q}\cdot\mathbf{H}|\right] + 2\lambda\mathbf{Q}|\mathbf{Q}\cdot\mathbf{H}| + [\mathbf{Q}\cdot\mathbf{H}]^A + \boldsymbol{\sigma}^E \,, \tag{75}$$

where $\mathbf{1}$ is the unite tensor. Here σ^e_{ij} represents the $i-$th component of the force exerted on a unit area of fluid element oriented with normal along the j direction. The last term in Eq. (75) is the Erickssen stress $\boldsymbol{\sigma}^E = -\boldsymbol{\nabla}\mathbf{Q} : \frac{\delta F}{\delta \boldsymbol{\nabla}\mathbf{Q}}$ included here for completeness but neglected in the following.

The importance of inertia described by the left hand side of the Navier-Stokes can be quantified in terms of the Reynold number defined as the ratio of inertial to dissipative forces as

$$\mathrm{Re} = \frac{\text{inertia}}{\text{viscous dissipation}} \sim \frac{v^2\rho/L}{\eta v L^2} = \frac{vL\rho}{\eta} \tag{76}$$

where L is a characteristic length scale. Many active systems are in a regime where the Reynolds number is very small and inertia can be neglected. In this limit, the Navier -Stokes equation is replaced by the Stokes equation that simply describes force balance as

$$-\boldsymbol{\nabla}P + \eta\nabla^2\mathbf{v} + \boldsymbol{\nabla}\cdot\boldsymbol{\sigma}^e = 0 \,. \tag{77}$$

For instance, for *E. coli* swimming in water $L \sim 3-5\mu m$, $v \sim 20-30\mu m$ and $\eta/\rho \sim$, which gives $Re \sim 10^{-5}$.

Finally, when the liquid crystal is a thin film in contact with a substrate that provides friction, momentum is no longer conserved. Such systems are generally in the Stokes limit, with

$$\Gamma\mathbf{v} = -\boldsymbol{\nabla}P + \eta\nabla^2\mathbf{v} + \boldsymbol{\nabla}\cdot\boldsymbol{\sigma}^e \,, \tag{78}$$

where $\Gamma = \zeta\rho$ is a friction per unit area, with ζ a friction. The presence of friction screens long-ranged hydrodynamic flows over a characteristic length scale $\ell_v = \sqrt{\Gamma/\eta}$.

Exercise 7.
Show that in two dimensions $Tr[\mathbf{Q}^3] = Q_{ij}Q_{jk}Q_{ki} = 0$ identically.

VI. ACTIVE NEMATICS LIQUID CRYSTALS

A. Active stress

These systems are collections of elongated active agents, such as bacteria or microtubule-kinesin bundles, that exert force dipoles on their surrounding, generating self-sustained flows. The active agents are apolar (essentially "shakers") and there is no mean flow at large scales. The continuum equations need to be modified to include the force density that the active agents exert on the fluid. Given the system is force-free, there is no mean force, and the first contribution in a multipole expansion of the force density takes the form of the gradient of an active stress. To understand the from of such a stress, consider a collection of identical and nonteracting active agents that exert force dipoles directed along their long axis, as shown in Fig. The force density that the agents impart on the fluid can be written as

$$\mathbf{F}^a(\mathbf{r},t) = \Big\langle \sum_n \left[f\hat{\boldsymbol{\nu}}_n\delta\left(\mathbf{r}-\mathbf{r}_n-\frac{L}{2}\hat{\boldsymbol{\nu}}_n\right) - f\hat{\boldsymbol{\nu}}_n\,\delta\left(\mathbf{r}-\mathbf{r}_n+\frac{L}{2}\hat{\boldsymbol{\nu}}_n\right)\right]\Big\rangle \,, \tag{79}$$

where $\mathbf{r}_n$ is the location of the center of the $n-$th active agent and L its the length. The brackets denote an average over a local region containing many agents. If we are interested in the behavior on length scales large compared to the agents' size, we can expand the argument of the δ functions, with the result

$$F_i^a(\mathbf{r},t) = \partial_j \Big\langle fL \sum_n \hat{\nu}_{ni}\hat{\nu}_{nj}\delta\left(\mathbf{r}-\mathbf{r}_n\right)\Big\rangle \; + \mathcal{O}(\nabla^2) \; , \tag{80}$$

It is clear that the right hand side of Eq. (80) can be related to the nematic order parameter. We can therefore define an active stress as

$$F_i^a \simeq \partial_j \sigma_{ij}^a \; , \tag{81}$$

where

$$\sigma_{ij}^a = \alpha Q_{ij} + \delta_{ij}\alpha'\rho \; . \tag{82}$$

Here α and α' have dimensions of stress and are controlled by the molecular mechanism that determine the force f generated by the active agents, as well as by their density. The simple estimate obtained here yields $\alpha = fl\rho$ and $\alpha' = fL\rho/2$. The sign of α and $alpha'$ is determined by the sign of the force dipole: $\alpha, \alpha' < 0$ correspond to extensile forces, as shown in the figure, while $\alpha, \alpha' > 0$ correspond to contractile ones. In the swimmer literature agents that exert extensile (contractile) forces are referred to as pushers (pullers).

The only modification of the continuum hydrodynamic for an active nematic as compared to a passive one is therefore the replacement of the elastic stress $\boldsymbol{\sigma}^e$ with the total stress $\boldsymbol{\sigma}^e + \boldsymbol{\sigma}^a$. It is then evident that distortion of orientational order act as sources of flow, which in turn rotates and advect the nematic director, resulting in self-sustained dynamics.

B. Active Nematohydrodynamics

To summarize, the hydrodynamic equations for an incompressible active nematic are given by

$$D_t\mathbf{Q} + [\boldsymbol{\Omega}\cdot\mathbf{Q}]^A = \frac{\lambda}{2}[\boldsymbol{\nabla}\mathbf{v} + (\boldsymbol{\nabla}\mathbf{v})^T] + \frac{1}{\gamma}\mathbf{H} \; , \tag{83}$$

$$\rho D_t\mathbf{v} = -\boldsymbol{\nabla}P + \eta\nabla^2\mathbf{v} + \boldsymbol{\nabla}\cdot\left(\boldsymbol{\sigma}^e + \boldsymbol{\sigma}^a\right) \; , \qquad \boldsymbol{\nabla}\cdot\mathbf{v} = 0 \; , \tag{84}$$

where the molecular field $\mathbf{H}$ is given by Eq. (**??**) and the elastic and active stresses are given by Eqs. (75) and (82), respectively. In the next few sections we show how active stresses drive director deformations that destabilize both the homogeneous isotropic and nematic states, leading to self-sustained flows.

C. Active nematics are always unstable

The homogeneous ordered state of an active nematic liquid crystal is linearly unstable for any finite activity. This result first demonstrated in 2002 in a seminal paper by A. Simha and S. Ramaswamy [83] is often referred to as the *generic instability* of active nematics is at the foundation of much of their behavior. The homoegenous isotropic state is also linearly unstable, but only above acritical value of activity. Frictional dissipation can stabilize both the isotropic and ordered states at low activity, but again the fluid becomes unstable above an activity threshold and develops spatio-temporal dynamics. In this section we examine this instability in some detail.

1. *Linear stability of the isotropic state*

We examine the linear stability of homogeneous, steady state solutions of Eqs. (**??**) to fluctuations $\delta\mathbf{Q} = \mathbf{Q} - \mathbf{Q}_0$ and $\delta\mathbf{v} = \mathbf{v} - \mathbf{v}_0$ of the continuum fields from their mean values. The isotropic state (for $a > 0$ has $\mathbf{Q}_0 = \mathbf{v}_0 = 0$. For generality we include substrate friction, but neglect inertia and simply use the Stokes equation for velocity fluctuations. We additionally work in the one-elastic constant approximation. Expanding the fluctuations in Fourier components as $\delta\boldsymbol{\psi}(\mathbf{r}, t) = \int_{\mathbf{q}} \hat{\boldsymbol{\psi}}_{\mathbf{q}}(t) e^{i\mathbf{q}\cdot\mathbf{r}}$, with $\psi = (\delta\mathbf{Q}, \delta\mathbf{v})$, the linearized equations take the form

$$\partial_t \hat{Q}_{ij} = i\frac{\lambda}{2}(q_i\hat{v}_j + q_j\hat{v}_i) - \left(\frac{1}{\tau_N} + \frac{K}{\gamma}q^2\right)\hat{Q}_{ij} \,, \tag{85}$$

$$\Gamma\hat{v}_i = -iq_i\hat{P} - \eta q^2\hat{v}_i + iq_j\left[\alpha + \lambda(a + Kq^2)\right]\hat{Q}_{ij} \,. \tag{86}$$

Given the system is isotropic, fluctuations transverse and longitudinal to $\mathbf{q}$ can be decoupled by letting

$$Q_\parallel = \hat{q}_i\hat{Q}_{ij}\hat{q}_j \qquad Q_\perp = \hat{q}_i\hat{Q}_{ij}\hat{q}^\perp_j \,, \tag{87}$$

$$v_\parallel = \hat{\mathbf{q}}\cdot\mathbf{v} = \hat{v}_i\hat{q}_i \qquad v_\perp = \hat{\mathbf{z}}\cdot(\hat{\mathbf{q}}\times\mathbf{v}) = \epsilon_{ij}\hat{q}_i\hat{v}_j \,, \tag{88}$$

where $\hat{\mathbf{q}} = \mathbf{q}/q$ and $\hat{\mathbf{q}}^\parallel = ...$ Incompressibility requires $v_\perp$, and we obtain

$$\partial_t Q_\parallel = -\left(\frac{1}{\tau_N} + \frac{K}{\gamma}q^2\right)Q_\parallel \,, \tag{89}$$

$$\hat{P} = \left[\alpha + \lambda(a + Kq^2)\right]Q_\parallel \,, \tag{90}$$

and

$$\partial_t Q_\perp = -\left(\frac{1}{\tau_N} + \frac{K}{\gamma}q^2\right)\psi_\perp + \frac{\lambda}{2}iqv_\perp \,, \tag{91}$$

$$(\Gamma + \eta q^2)v_\perp = iq\left[\alpha + \lambda(a + Kq^2)\right]Q_\perp \,. \tag{92}$$

The parallel component $Q_\parallel$ relaxes on the nematic time scale τ_N and Eq. (90) determines the pressure. By eliminating $v_\perp$ (which is directly related to the vorticity of the flow) from Eq. (91) we can immediately read off the relaxation rate of $Q_\perp$ as

$$s(q) = -\left[\frac{1}{\tau_N} + \left(\frac{K}{\gamma} + \frac{\lambda}{2}\frac{\alpha + \lambda(a + Kq^2)}{\eta q^2 + \Gamma}\right)q^2\right] \tag{93}$$

The homogeneous isotropic state will be unstable whenever $\sigma(q) > 0$ for some q. This is possible when $\lambda\alpha < 0$, i.e., for either extensile systems with $\lambda > 0$ (i.e., nematogens that tend to align with the flow) or contractile systems with $\lambda < 0$ (i.e., nematogens that tend to align with flow gradients). The dispersion relation is plotted in Fig. **??**, which shows that the nature of this activity-driven instability depends on the interplay frictional and viscous frictional dissipation.

Exercise 7.
Using Eq. (93), find the threshold values of activity for the instability and the wavenumber of the most rapidly growing mode.

2. Linear stability of the nematic state

Deep in the nematic state fluctuations in the magnitude S of the nematic order parameter relax quickly and one can simple examine the dynamics of the director field coupled to flow. Furthermore, we rescale parameters so that $S_0 = 1$ and choose the x direction as the direction of broken symmetry. We additionally consider the Stokes limit, where the left hand side of Eq. (84) can be set equal to zero. The equation for the director field is then given by

$$\mathcal{D}_t n_i + \Omega_{ij} n_j = \lambda E_{ij} n_j + \frac{h_i}{\gamma} \,, \tag{94}$$

$$h_i = (K_1 - K_3)\partial_i \boldsymbol{\nabla} \cdot \mathbf{n} + K_3 \nabla^2 n_i + h_\parallel n_i \,, \tag{95}$$

where we have included in the free energy a Lagrange multiplier $h_\parallel$ to enforce the constraint $|\mathbf{n}| = 1$. Fluid flow in the Stokes limit is controlled by force balance, $\partial_j \sigma_{ij} = 0$, with

$$\sigma_{ij} = 2\eta E_{ij} - (P - \alpha_B)\,\delta_{ij} + \alpha\left(n_i n_j - \frac{1}{2}\delta_{ij}\right) - \frac{\lambda}{2}(n_i h_j + n_j h_i) + \frac{1}{2}(n_i h_j - n_j h_i) \tag{96}$$

We now linearize these equations about an ordered and quiescent homogeneous state by letting $\mathbf{n} = \hat{\mathbf{x}} + \hat{\mathbf{y}}\delta n_y$ and $\mathbf{v} = 0 + \delta\mathbf{v}$. The constraint $|\mathbf{n}| = 1$ requires director fluctuations to only have components in the y direction to linear order. Also, we can drop $h_\parallel$ to linear order.

Letting $\delta n_y = \theta$, we find

$$\partial_t \hat{\theta} = \frac{\lambda - 1}{2} i q_y \hat{v}_x + \frac{\lambda + 1}{2} i q_x \hat{v}_y - \frac{1}{\gamma}(K_1 q_y^2 + K_3 q_x^2)\hat{\theta} \tag{97}$$

$$[\Gamma + \eta q^2]\hat{v}_x = i q_y \left[\frac{\lambda - 1}{2}(K_1 q_y^2 + K_3 q_x^2) + \lambda(K_1 - K_3) q_x^2 + \alpha\right]\hat{\theta} - i q_x \hat{P} \tag{98}$$

$$[\Gamma + \eta q^2]\hat{v}_y = i q_x \left[\frac{\lambda + 1}{2}(K_1 q_y^2 + K_3 q_x^2) + \alpha\right]\hat{\theta} - i q_y \hat{P} \tag{99}$$

We can solve for pressure by imposing incompressibility. Taking again the one-elastic constant approximation $K_1 = K_3 = K$, we obtain the growth rate of director fluctuations as [84, 85]

$$\sigma_N(q) = -\frac{\alpha q^2 \cos 2\phi(1 + \lambda \cos 2\phi)}{2(\Gamma + \eta q^2)} - \frac{K q^2}{\gamma}\left[1 + \frac{\gamma q^2 (\lambda \cos 2\phi + 1)^2}{4(\Gamma + \eta q^2)}\right] \tag{100}$$

MCM: must check the factor in the second term. where ϕ is the angle between $\mathbf{q}$ and the nematic director. The quartic term is always negative, as required by stability at short wavelengths. When friction with the substrate is neglected the dispersion relation simplifies to

$$\sigma_N(q)|_{\Gamma=0} = -\frac{\alpha}{2\eta}\cos 2\phi(1 + \lambda \cos 2\phi) - \frac{K}{\gamma} q^2 \left[1 + \frac{\gamma}{4\eta}(1 + \lambda \cos 2\phi)^2\right] \tag{101}$$

The growth rate depends on the angle ϕ between the wave vector of the diretcion of broken symmetry. When $\phi = 0$ the fluctuations are along the direction of alignment ($\partial_x \delta n_y \neq 0$), correponding to bend deformations of the director field. In this case, the ordered state is unstable if $\alpha(1 + \lambda) < 0$. This corresponds to extensile stresses ($\alpha < 0$) for rod-like systems ($\lambda > 0$) and contractile stresses ($\alpha > 0$) for prolate flow-aligning particles ($\lambda < -1$). For $\phi = \pi/2$ the fluctuations are perpendicular

to the direction of order ($\partial_y \delta n_y \neq 0$) and correspond to splay distortion of the director field. In this case, the instability occurs for $\alpha(1-\lambda) < 0$, corresponding to contractile stresses for rod-like nematogens ($\lambda > 1$). In other words, rod-like extensile nematics, as realized in microtubule-kinesin suspensions, are always unstable to bend fluctuations. A plot of the instability regions in the (α, λ) plane is shown in Fig. 13.

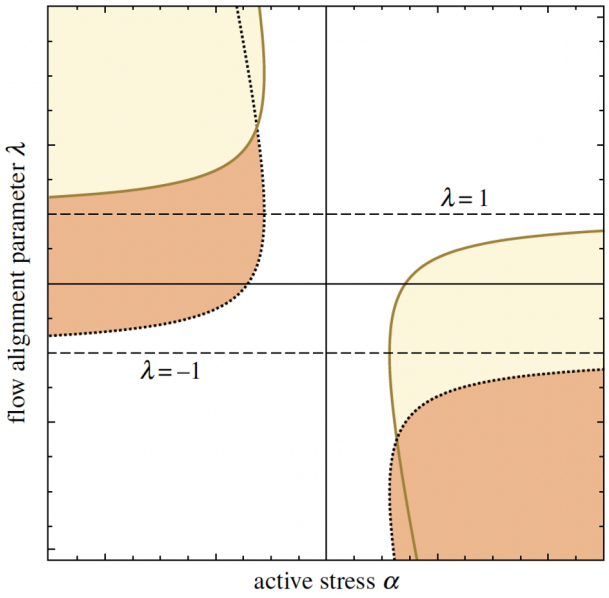

Figure 13. Schematic of the regionwhere an active nematic is linearly unstable to splay (yellow/light) and to bend (orange/dark) fluctuations in the plane of the alignment parameter λ and the activity α. From [84].

Exercise 8.
(a) Derive Eq. (101) and discuss the mechanisms for instability in the cases $\Gamma = 0$ and $\eta = 0$.
(b) Plot the dispertion relations for a few parameter values (e.g., a few values of activity.

D. Spontaneous flow

The generic instability of active nematic also implies that, when confined to a channel, an active nematic liquid crystal will spontaneously exhibit laminar flow, with no externally applied forces. This remarkable result, first predicted by Voituriez *et al.* in 2005 [86], has been verified experimentally in both confined monolayers of living cells [85] and microtubule-kinesin suspensions.

The onset of spontaneous flow can be understood physically by a simple force balance argument. We consider a quiescent layer of active nematic in the configuration of Fig. 14. In the absence of external forces, the system must satisfy $\partial_x \sigma_{yx} = 0$ (the pressure is controlled by incompressibility). This requires σ_{yx} to be a constant, which can be taken equal to zero given there are no externally

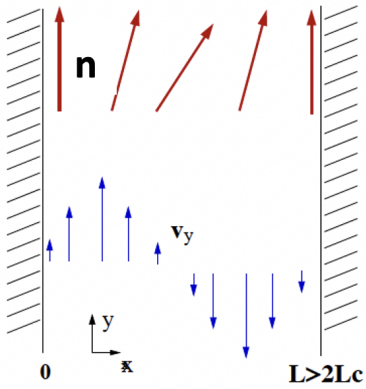

Figure 14. Schematic of an active nematic in a channel showing the onset of spontaneous flow for no slip boundary consitions on the velocity. From [86].

applied forces. In other words, force balance requires

$$\sigma_{yx} = \eta \partial_x v_y + \frac{\alpha}{2} \sin 2\theta - \frac{\lambda}{2} \partial_x^2 \theta = 0 \tag{102}$$

where θ is the director angle. It is then evident that the system can satisfy force balance by selecting a configuration that balances elastic deformations of the director field with a non-zero flow profile. The characteristic length scale that balancles elastic and active stresses is $\ell_\alpha = \sqrt{K/|\alpha|}$. The steady state is then controlled by the ratio of the channel width to the active length as follows

$L < \ell_\alpha$	$L > \ell_\alpha$	$L \gg \ell_\alpha$
anchoring & elasticity win	spontaneous	chaotic flow,
$\rightarrow$ no flow	laminar flow	"active turbulence" + defects

These regimes are seen in microtubule nematics and cell monolayers, where a quantitative comparison has been carried out [85] (Fig. 15).

Finally, it has been shown that contractile active stresses sources by nematically ordered myosin act as a source of flow in the *Drosophila* embryo during gastrulation. By independently measuring the myosin pattern (a nematic tensor) and the cellular flows, Streichan *et al.* (*eLife* 2019) showed that anisotropic myosin stresses with dorso-ventral nematic alignment drive the flows observed during gastrulation, validating the active matter model *in vivo*.

E. Motile topological defects

In both passive and active liquid crystals, distortions of orientational order generate flows, and flows in turn deform the ordered state. The key distinction between passive and active systems is that in the former, flows and deformations are generated by applying external fields or via boundary

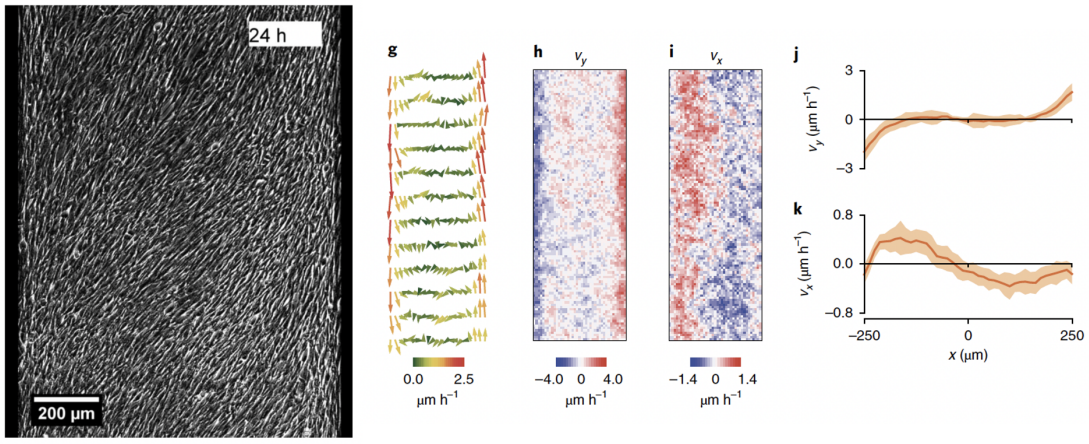

Figure 15. Quantification of observed spontaneous flow ina layer of elongated retinal pigment epithelial cells (left) showing the local velocity field (g) heat maps of v_y and v_x (h,i), and line plots of the $y-$averaged velocity components (j)From [85].

conditions. Such flows are transient: the system always relaxes to the equilibrium (ordered) state upon removal of perturbations or constraints. In active systems, in contrast, flows and deformations are internally generated and self-sustained. In 2D, bulk active nematics are generically unstable to bend or splay deformations generated by local active fluctuations [83]. As these distortions grow in time, they generate flows that further enhance the deformations, ultimately generating unbound pairs of topological defects. Such spontaneously generated defects are themselves strong distortions of orientational order and yield distinctive flow patterns [87, 88]. This intimate connection between defects and flows, offers the opportunity to direct and localize nonlinear active flows by controlling the dynamics of topological defects [89–91].

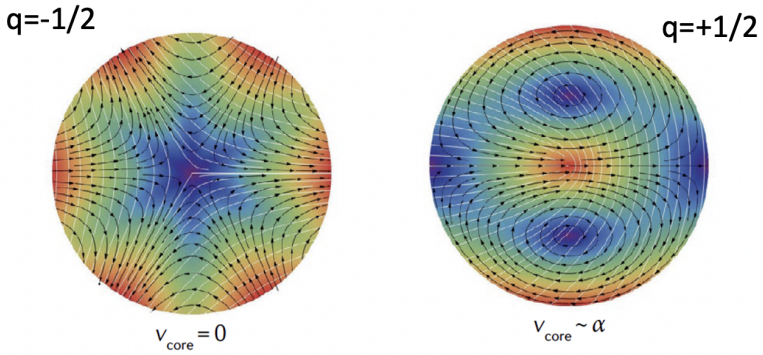

Figure 16. Flow field generated by half-integer defects.

In 2D active nematics, the comet-like $+1/2$ defect (see Fig. 16) generates a flow that is finite at the defect core. The $+1/2$ defect then rides along with the flow it generates, behaving like a self-propelled polar particle [87, 92]. In contrast, the flow generated by a $-1/2$ defect vanishes at the defect core due to the defect's threefold symmetry (see Fig. 16), and to leading order in activity this defect remains a "passive" particle.

One can calculate the flow due to a defect (or backflow) by solving a simplified version of the Stokes equation that neglects liquid crystalline elastic stresses,

$$\eta\nabla^2\mathbf{v} - \boldsymbol{\nabla}p + \mathbf{f}^a \,, \qquad \boldsymbol{\nabla}\cdot\mathbf{v} = 0 \,, \tag{103}$$

where $\mathbf{f}^a = \boldsymbol{\nabla}\cdot\boldsymbol{\sigma}^a$ is the active forcing. Taking $\mathbf{n} = (\cos q\phi, \sin q\phi)$, with $q = \pm\frac{1}{2}$, the active force due to a defect is given by

$$\mathbf{f}^a = \frac{\alpha}{2r}\begin{cases} \hat{\mathbf{x}} & q = +\frac{1}{2} \\ -\cos 2\phi\hat{\mathbf{x}} + \sin 2\phi\hat{\mathbf{y}} & q = -\frac{1}{2} \end{cases} \tag{104}$$

The solution to the Stokes equation (103) can be written as

$$v_i(\mathbf{r}) = \int d\mathbf{r}' G_{ij}(\mathbf{r}-\mathbf{r}')f_j(\mathbf{r}') \tag{105}$$

where G_{ij} is the Oseen tensor. In $2D$ it is given by

$$G_{ij}(\mathbf{r}) = \frac{1}{4\pi\eta}\left[\left(\log\frac{L}{r} - 1\right)\delta_{ij} + \frac{r_i r_j}{r^2}\right] \tag{106}$$

Here L is a length scale chosen to obtain the right behavior at the boundary. A naive calculation for isolated defects yields

$$\mathbf{v}_+(r,\phi) = \frac{\alpha}{12\eta}\left\{[3(R-r) + r\cos 2\phi]\hat{\mathbf{x}} + r\sin 2\phi\hat{\mathbf{y}}\right\} \tag{107}$$

$$\mathbf{v}_-(r,\phi) = \frac{\alpha r}{12\eta R}\left\{\left[\left(\frac{3}{4}r - R\right)\cos 2\phi - \frac{R}{5}\cos 4\phi\right]\hat{\mathbf{x}} + \left[\left(\frac{3}{4}r - R\right)\sin 2\phi + \frac{R}{5}\sin 4\phi\right]\hat{\mathbf{y}}\right\} \tag{108}$$

Here $\mathbf{v}_-(0) = 0$ and $\mathbf{v}_+(0) = v_0\hat{\mathbf{x}}$. We find $v_0 = \alpha R/(4\eta)$, which we identifying with the defect velocity. Note that this velocity diverges with the system size R. In a system with many defects, R can be identified with the mean defect separation, which is turn is controlled by the active length $\sim\sqrt{K/|\alpha|}$. A calculation incorporating both viscous and frictional dissipation (as often appropriate for microtubule nematics) was carried out in Ref. []. Friction cuts off the large scale divergence and yields $v_0 \sim (\alpha/\eta)\ell_v$, where $\ell_v = \sqrt{\eta/\Gamma}$ is the screening length of the flow.

The cutoff does not change the symmetry of the active backflow. In all cases one finds that the direction of motion of the $+1/2$ defect is determined by its local orientation or polarity and by the sign of the active forcing. In extensile fluids ($\alpha < 0$), $+1/2$ defects actively propel themselves along the head of the comet, while in contractile systems ($\alpha > 0$) the active propulsion is directed along the comet's tail.

If chiral active stresses are present, $+1/2$ disclinations self-propel instead at an angle relative to their polarity [93, 94], and intrinsic active spinning renders defect trajectories circular [93]. In polar fluids, charge $+1$ spiral vortices undergo spontaneous rotation [42] due to the chirality of their spiral texture. Other low charge defects, such as circularly symmetric asters and antivortices,

perform neither rotational nor translational spontaneous motion. In contrast to defect motion in externally driven systems, the motion of active defects is dictated by the local *geometry* of the defect itself and not by a fixed external field, as would be the case, for example, for driven vortices in a superconducting film. This profound distinction leads to a plethora of phenomena characteristic of active matter.

Exercise 9.
Use Eqs. (107) and (108) to plot the flow field generated by topological defects.

F. Active turbulence

Beyond the instability threshold (which is zero for the nematic state) active liquid crystals exhibit self-sustained spatiotemporal chaotic flow that has been dubbed "active turbulence" [88, 95, 96]. This type of flow has been observed in a variety of systems, from suspensions of cytoskeletal filaments and motor proteins to bacteria, sperm cells, and cell layers. Unlike inertial turbulence which occurs at high Reynolds numbers, active turbulence occurs even when inertial effects are negligible (i.e., at essentially zero Reynolds number) and is akin to elastic turbulence in sheared polymer suspensions, where nonlinear elastic forces can destabilize the laminar flow. An important distinction is that in both inertial and elastic turbulence the scale at which energy is injected is imposed by the external driving. In active turbulence energy is injected internally and the flow pattern is self-organized.

In inertial turbulence energy is injected from the outside at large scales and transported across scales through a process called energy cascade, until it is dissipated at small scales by viscous effects that turn it into heat. At intermediate scales, the flow is self-similar and the energy spectrum of the flow exhibits a characteristic power-law scaling as a function of wave number predicted by Kilmogorov in 1941, $E(q) \sim q^{-5/3}$, with a universal exponent.

In active systems, various scaling exponents have been observed for the energy spectrum in both experiments and simulations, depending on the symmetry of the system (polar vs nematic) and on the relative importance of frictional vs viscous dissipation. The phenomenology and scaling properties of active turbulence have been detailed in a recent review [96]. Here we focus on its topological aspects and sketch the physical arguments underpinning the unbinding of active defects [97].

Active turbulence is characterized by vorticity and shear flows on a typical length scale that controls the mean defect separation and is set by a balance of active and elastic stresses [88, 98–101]. In a 2D active nematic, an isolated $\pm 1/2$ disclination pair continues to experience the passive attractive force $\sim K/r$ from elasticity, but in addition, for certain configurations, such as the one shown in Box 1, the $+1/2$ defect can propel itself with speed $\sim v_0$ away from the $-1/2$ defect. One can then argue that, neglecting inertia, the pair dynamics of active defects is governed by relaxation in a an effective potential [87],

$$\dot{r} = -\mu \partial_r V \ , \quad V(r) = \frac{\pi K}{2} \ln\left(\frac{r}{a}\right) - \frac{v_0}{\mu} r \ , \tag{109}$$

where a may be taken to be the defect core size. The resulting barrier

$$V(r_c) = \frac{\pi K}{2}\left[\ln\left(\frac{\pi \mu K}{2 v_0 a}\right) - 1\right] \tag{110}$$

at distance $r_c = \pi \mu K/(2v_0)$ is finite, which means that the defect pair is always unbound, and active nematic order thus destroyed, at any nonzero temperature (Fig. 17). As activity is increased,

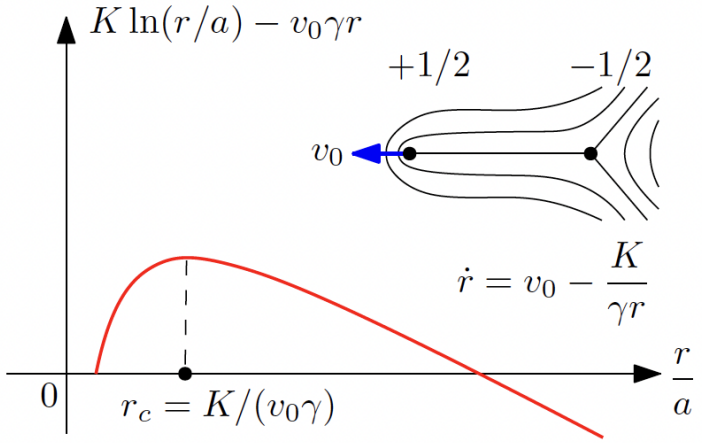

Figure 17. Effective potential for a neutral defect pair for the configuration in which the direction of motility of the $+1/2$ disclination is held fixed and pointed away from the $-1/2$

more and more defect pairs will be liberated and subsequently annihilated [7, 87, 102]. One might then expect that nematic order would be completely destroyed by the swarming disordered cores, much like driven vortices in high-temperature superconducting films can destroy superconductivity.

This heuristic argument, however, fails because $+1/2$ defects do not travel in a straight line, rather their direction of motion is affected by rotational noise and changes in the local nematic structure. Unlike the motion of charges driven by an externally applied electric field, the motility of $+1/2$ disclinations is determined by their local geometry. As a result, the $+1/2$ defect has a finite persistence length $\ell_p = v_0\tau_R$ beyond which its motion is not ballistic, where τ_R^{-1} controls the rate of rotational noise from active processes. Upon comparing this persistence length to the length scale r_c where pair attraction and defect propulsion balance, we get a simple criterion for active defect unbinding [97]. Defect pairs unbind if $\ell_p > r_c$. Conversely, when $\ell_p < r_c$, the $+1/2$ defect changes its direction of motion before overcoming Coulomb attraction, resulting in a local change of the nematic texture that allows the pair to remain bound. It is interesting to note that rotational noise here stabilizes the quasi-ordered nematic phase below a finite activity threshold by disrupting the persistent motion of the $+1/2$ defect. This order-from-disorder mechanism highlights the difference between active and driven defects: the latter would inevitably unbind under the action of any external field as nothing disrupts their straight line motion. This argument can be made systematic by constructing Langevin equations for the dynamics of the positions $\underline{\mathrm{r}}_i^{\pm}$ of the $\pm 1/2$ defects and the orientation $\underline{\mathrm{e}}_i$ of the $+1/2$ defects, starting from the continuum hydrodynamic equations of a $2d$ dry active nematic [89, 97].

Above a critical value of activity, the BKT-like unbinding yields an interacting gas of unbound and swarming defects that provides a useful picture to describe the state of active turbulence. Several models of varying complexity have been proposed for the dynamics of active defects [87, 92, 97, 103–108]. While details differ, the basic physics is the same: the unbound defect gas is a mixture of self-propelled (the $+1/2$ defects) and passive (the $-1/2$ defect) charged particles interacting via Coulomb forces. Recent work has also emphasized the non-reciprocal nature of active defect interactions [108, 109], although much remains to be explored. Coarse-graining over many defects

allows a hydrodynamic description of the active defect gas [89, 110], along the lines of previous classic works in the context of superfluid vortices [111] and 2D crystal melting [112]. Importantly, a hydrodynamic treatment of defects offers a theoretical handle on the strongly interacting many-body dynamics of this far-from-equilibrium system. As a crucial ingredient, this description includes a polarization field that captures the average orientation of a collection of active $+1/2$ defects. This field accounts not only for self-propulsion actively driving material flow, but being a vector, the orientation also experiences active torques. When activity is sufficiently strong, and viscous stresses are negligible compared to frictional dissipation with a substrate, one finds that the $+1/2$ defects spontaneously condense into a polar-ordered collectively moving state—a defect flock [89]. Heuristically, such a state arises when the underlying nematic elasticity is too slow to relax the distortion created in the wake of an unbinding defect pair. Similar defect-ordered states have been observed previously in simulations, either with polar ordering [113–116] or defect lattices [117]. Experiments on microtubule-kinesin based active nematic films have reported an extraordinary *nematic* ordered defect state [113]. While continuum simulations recover largely transient nematic defect ordering [115, 118], this observation continues to be a theoretical puzzle. Recent work suggests that elastic torques may play a role in antipolar ordering of defects [119, 120].

VII. NEMATIC ORDER IN BIOLOGY

Nematic order in biological context was reported by T.R. Elsdale back in 1968 when he described a monolayer of elongated fibroblasts as a "patchwork of aligned groups of parallel cells with narrow interstices between them that we term *frontiers*." What Elsdale called frontiers are what we now identify as topological defects. Since then, nematic order has been observed ubiquitously in biological systems on many scales. This ranges from the alignment of stress fiber in the interior of a single cell to the organization of myosin across cells in the developing fruit fly embryo, cell monolayers, and even entire organs and organisms. There are some recent reviews focused on biological relevance of nematic order, such as Refs. [9, 10], where one can find many relevant references. An especially exciting development has been the demonstration of the relevance of topological defects for specific biological functions. In general defects can fucus stresses and strain, hence can driven morphogenetic changes of the tissue. Topological defects in monolayers of epithelial cells [78] and of spindle-shaped neural stem cells [77] have been correlated with cell extrusion and cell death. In these systems cells preferentially accumulate at $+1/2$ defects and deplete the core region of $-1/2$ defects. This behavior originates from the large distortion of order around the defect which generates strong local active stresses. These large compressive stresses ultimately lead to cell extrusion and death in epithelia [78]. The structure and role of these active stresses has been confirmed by direct traction force microscopic measurements and via comparison with simulations of active nematic hydrodynamics. Similar phenomena have now been reported in bacterial systems as well. In growing biofilms, $-1/2$ defects instead provide sites for mound formation and buckling [81], while geometrically patterned $+1$ asters have been suggested to support the formation of vertical finger-like structures that extrube form the monolayer [82]. Motile bacteria also display related behaviour; for instance, starved myxobacteria use $\pm 1/2$ defects to seed multilayers and cavities to initiate fruiting body formation [79], while slow moving *P. aeruginosa* cells outcompete faster mutants that effectively jam at defects and escape into the third dimension [80].

The role of defects in morphogenesis has been demonstrated in the development of *Hydra*, a freshwater polyp capable of regenerating itself from a fragment. The "skin" tissue of *Hydra* consists of two cell layers (ectoderm and endoderm) separated and connected by ECM. Supracellular actin fibers (referred to below as "muscle fibers") align orthogonal to each other, with fibers in the

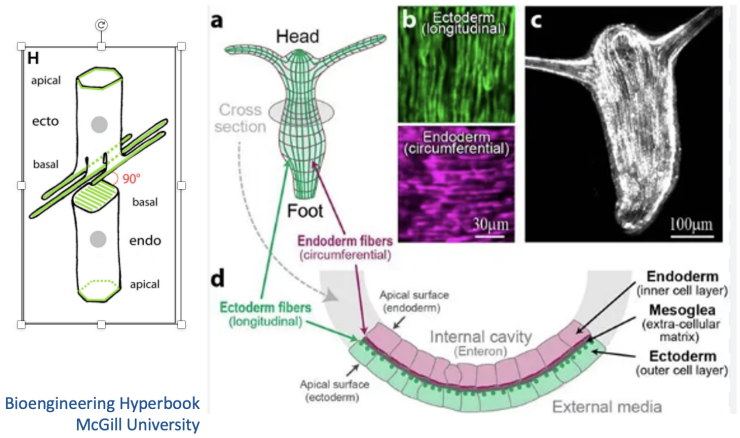

Figure 18. Structure of the frshwater polyp Hydra.

ectoderm aligned along the long direction of the body axis and those in the endoderm aligned circumferentially. During regeneration, while this nematic structure develops, defects are generated. Given the organism has the topology of a sphere, the adult structure must contain a net topological charge +2. In this organism a correlation has been established between the location and structure of topological defects. As discussed in the next section, however, there is strong evidence that the muscle fibers in *Hydra* behave more like an elastic solid than a liquid on the time scale of experiments (no appreciable cell intercalation nor division is observed during regeneration).

VIII. ACTIVE NEMATIC SOLIDS

Passive nematic elastomers have been studied extensively. In these materials topological defects can be used to control shape morphing through forces generated via chemical or thermal activation of the elastomer. These forces yield nemato-elastic stresses that deform the system [121–123]. Theoretical studies of such shape-morphing solids have focused on quantifying the deformations induced by prescribed ("frozen-in") nematic textures [124–127].

In certain situations, and for a range of time scales, biological tissues behave more like solids than like liquids. This has motivated interest in understanding the interplay between nematic texture, elasticity and active forces, leading to the formulation of models of active elasto-nematics. An additional ingredient in these biological tissues is biochemical signaling, in the form of expression of morphogens described by scalar concentration fields that can activate or inhibit mechanical processes. for instance, On the other hand, *Hydra's* body plan is known to be organized by the concentration profiles of a specific class of morphogens [128–130]. Specifically, experiments indicate that muscle fibers in *Hydra* might align along gradients in a central player of the Wnt-morphogen pathway that sets Hydra's up the head-to-foot body axis [131, 132]. While the molecular mechanism underlying this coupling remains to be investigated, these experiments suggests that alignment of fibers along morphogen gradients may drive the reorganization of their orientation during key morphogenetic processes, such as body-plan development and budding. [73, 132–135]. Some of the questions addressed are: Can nematic order emerge through coupling to mechanical strains or

stresses? What is the relative role of geometry, biochemical signaling and mechanics in driving structure and shape? How can defects move in an active nematic solid?

As a first step, we examine the behavior of planar elastonematics. Both models where the nematic tensor $\mathbf{Q}$ couples to the total stress (elastic plus active) or to the elastic stress or strain only have been considered in different settings.

A. Defect motility and unbinding in active solids

A direct generalization of passive nematic elastomers is obtained by coupling $\mathbf{Q}$ to the elastic strain tensor $u_{ij} = (\partial_i u_j + \partial_j u_i)/2$, where $\mathbf{u}$ is the deformation field. Here and below we will use tilde to denote the deviatoric part of tensors, e.g., $\tilde{u}_{ij} = u_{ij} - \frac{1}{2}\delta_{ij}u_{kk}$). The free energy includes the usual Landau–de Gennes term for the isotropic–nematic transition, Frank elastic coupling in the single elastic constant K approximation, and linear elasticity parametrized by the shear modulus μ and the bulk modulus B:

$$\mathcal{F} = \mathcal{F}_{LdG} + \mathcal{F}_e + \mathcal{F}_\chi \,, \tag{111}$$

$$\mathcal{F}_{LdG} = \frac{1}{2}\int \mathrm{d}\mathbf{r}\left[aQ_{ij}Q_{ij} + b(Q_{ij}Q_{ij})^2 + K(\nabla_i Q_{jk})^2\right] , \tag{112}$$

$$\mathcal{F}_e = \frac{1}{2}\int \mathrm{d}\mathbf{r}\left[2\mu\tilde{u}_{ij}\tilde{u}_{ij} + Bu_{kk}^2\right] , \tag{113}$$

$$\mathcal{F}_\chi = -\frac{1}{2}\int \mathrm{d}\mathbf{r}\left[\chi_B u_{kk}Q_{ij}Q_{ij} + 2\chi\tilde{u}_{ij}Q_{ij}\right] . \tag{114}$$

We begin by examining the behavior in the nematic state. Hence we choose $a = -1$ and $b = 1$ so that $2Q_{ij}Q_{ij} = S^2 = 1$ for the uniform equilibrium when $\chi = \chi_B = 0$. The coefficient χ accounts for strain alignment of nematic order along the direction of deviatoric strain $\tilde{u}_{ij}$, aligning them when $\chi > 0$ and anti-aligning them for $\chi < 0$. The strain alignment term can be derived by linearizing the Warner–Terentjev model for nematic elastomers [121]. It leads to a soft mode since the elastomer can accommodate shear through reorientation of the nematic [136]. In biological tissue, cytoskeletal nematic order has been found to align along the principal cell stretch axis [**?** **?**]. The coefficient χ_B describes the coupling of the nematic order to isotropic strain u_{kk}. We call this "strain ordering." For $\chi_B > 0$, nematic order decreases ("melts") in regions of compressive strain ($u_{kk} < 0$). Note that most passive nematic elastomer theories assume incompressibility, hence do not include this term.

In most biological tissue the nematic texture remodels on a time scale much slower (hours) than that of force equilibration through deformations (seconds to minutes). We therefore assume that the nematic texture evolves through relaxational dynamics to minimize the free energy, while elasticity is governed by force balance

$$\gamma\partial_t Q_{ij} = -\frac{\delta\mathcal{F}}{\delta Q_{ij}} \tag{115}$$

$$\partial_i\sigma_{ij} = 0 \,, \tag{116}$$

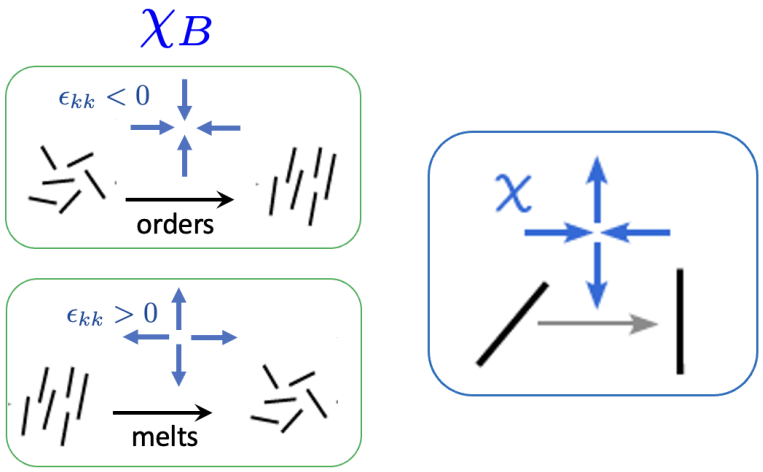

Figure 19. Schematic of the effect of the χ and χ_B couplings in Eq. (111) for $\chi_B < 0$.

where γ is the rotational viscosity. The total stress is

$$\sigma_{ij} = \sigma_{ij}^{\rm el} + \sigma_{ij}^{\rm a} \,, \tag{117}$$

$$\sigma_{ij}^{\rm el} = \frac{\delta \mathcal{F}}{\delta u_{ij}} = 2\mu u_{ij} - \chi Q_{ij} + \left[(B-\mu) u_{kk} - \frac{\chi_B}{4} S^2 \right] \delta_{ij} \,, \tag{118}$$

$$\sigma_{ij}^{\rm a} = \frac{\alpha_B}{4} S^2 \delta_{ij} + \alpha Q_{ij} \,. \tag{119}$$

We neglect passive stresses due to the nematic molecular field which are higher order in gradients than the active nematic stresses. We also assume a stiff elastic material, such that displacements are small, allowing us to neglect convective and co-rotational terms.

This model can be used to demonstrate a new mechanism for motion of $+1/2$ defects that occurs via texture restructuring with no material transport. We consider a single $+1/2$ defect with its tail pointing along the direction $\hat{\mathbf{p}} = \hat{\mathbf{x}}$ and centered at the origin. The associated $\mathbf{Q}$ is

$$\mathbf{Q}_{+\frac{1}{2}}(\mathbf{r}) = \frac{1}{2} S_{1/2}(r) \begin{pmatrix} \cos\theta & \sin\theta \\ \sin\theta & -\cos\theta \end{pmatrix} \,, \tag{120}$$

where (r, ϕ) denote polar coordinates. Equation (120) describes the "unperturbed" equilibrium texture of a $+1/2$ defect with $\chi = \chi_B = 0$. The magnitude of order $S_{1/2}(r)$ vanishes at the defect core $r = 0$ and is 1 for $r \gg \sqrt{K}$ with a transition zone (core size) of width $\sim \sqrt{K}$ (An approximate solution for $S_{1/2}(r)$ can be found using the Pad'e approximant

For simplicity we consider the case of purely deviatoric active stress ($\tilde{\alpha}_B = 0$). Taking the divergence of the force balance equation, $\partial_i \sigma_{ij} = 0$ gives an equation for the isotropic strain

$$(B+\mu) \nabla^2 u_{kk} = -\tilde{\alpha}\, \partial_i \partial_j Q_{ij} \,, \tag{121}$$

where $\tilde{\alpha} = \alpha - \chi$. For $\mathbf{Q} = \mathbf{Q}_{+\frac{1}{2}}$ Eq. (121) has the approximate solution

$$u_{kk}^{+\frac{1}{2}}(\mathbf{r}) \approx -\frac{\tilde{\alpha} S_{1/2}(r)}{2(B+\mu)} \frac{x}{r} \,. \tag{122}$$

For contractile active stress ($\tilde{\alpha} > 0$) this strain field is tensile in front of the defect and compressive behind it. In our model, this strain gradient leads to a free energy density gradient across the defect through the strain-ordering coupling χ_B. Thus, remodeling of the nematic texture propels the defect in the direction that reduces this free energy. As the defect moves, the strain field generated by active stresses shifts along with it such that there will always be a strain gradient across the defect core, sustaining the effective force acting on the defect. This propulsion mechanism is markedly different from the fluid case, where the defect is advected by the velocity field it actively induces.

The defect propulsion velocity can be estimated with a variational ansatz $\mathbf{Q}(\mathbf{r}, t) = \mathbf{Q}_{+\frac{1}{2}}[\mathbf{r} - \mathbf{r}_0(t)]$. The calculation is somewhat lengthy and requires numerical integration. It will not be repeated here (but see SI of Ref. []). One finds

$$\mathbf{v}_0 \approx 0.4 \, \frac{\tilde{\alpha} \chi_B \sqrt{K}}{\gamma_{+\frac{1}{2}}(B+\mu)} \, \hat{\mathbf{p}} \,. \tag{123}$$

with $\gamma_{+\frac{1}{2}}$ an effective friction. Importantly, the direction of propulsion of the $+1/2$ defect is determined by both the sign of the active stress α and that of the coupling parameter χ_B. In particular, this allows a system with contractile activity to have a defect move towards its head when χ_B is negative, i.e. when extensile strain reduces nematic order. This is in contrast to active fluids, where the sign of activity alone controls the direction of propulsion such that $+1/2$ defects move towards their tail for contractile activity.

These mechanisms may provide an explanation for a puzzling observation in cell monolayers, where defect motion often suggests extensile activity despite contractile forces at the cell scale [78, 137, 138]. Several explanations have been proposed [139–142], including most recently that cell motion is primarily driven by propulsive traction with the substrate and that the nematic texture of cell shapes and associated topological defects is a passive response [143, 144]. The mechanism proposed here provides an alternative explanation that does not require cell motility. The telltale sign of this mechanism is that defects move relative to the cells, as it is observed in regenerating *Hydra* [73]. To investigate this one will need simultaneous tracking of topological defects and individual cells.

This model can also account for defect pair unbinding via a mechanism similar to that studied in Ref. [87] for active fluids. For details see Ref. [].

Of course in-plane stress can also drive out-of-plane deformations, generating 3D shapes [124, 145]. Investigating the interplay of dynamic topological defects and 3D shape change is an important future direction with applications from morphogenesis and tissue engineering to soft robotics.

B. Role of morphogen

In *Hydra*, as well as in other developmental settings, coupling between stress and nematic order might be mediated by intermediary biochemical processes and signaling molecules (morphogens). One can show that coupling to morphogen concentration gradients can provide additional mechanisms for defect unbinding and propulsion [**?**].

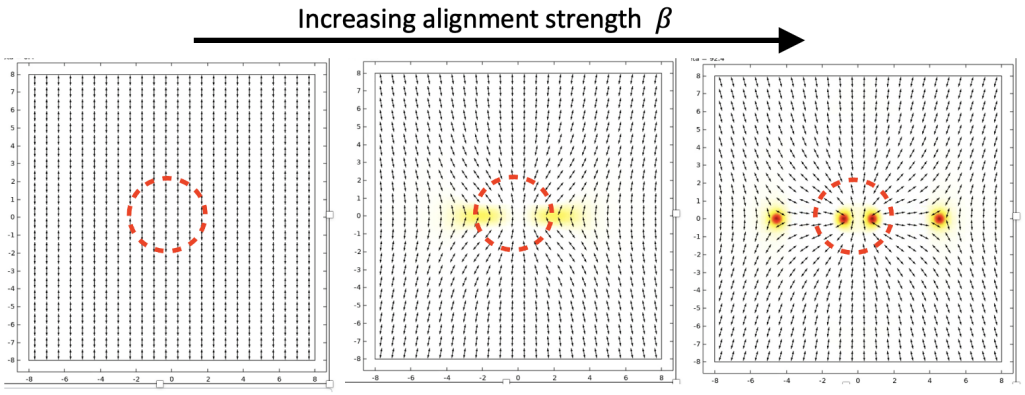

Figure 20. Alignment to morphogen gradients drives the unbinding of two $\pm 1/2$ defect pairs in an intially uniform planar nematic. The snapshots correpsond to inccreasing values of β. The left image is for $\beta = 0$. The dashed red circle if the location of maximum concentration gradient. the background color is magnitude of nematic order, with white correpsondign to $S = 1$ and yellow to lower values of S.

In the simplest model one can start by examining the interplay between nematic elasticity and a prescribed profile of morphogen described by a concentration field $c(\mathbf{r})$. Working again in a planar geometry, the free energy can be written as

$$\mathcal{F} = \mathcal{F}_{LdG} + \mathcal{F}_m \ , \tag{124}$$

where $\mathcal{F}_{LdG}$ is again the Landau-de Gennes free energy given in Eq. (**??**) and the coupling the morphogen gradients is given by

$$\mathcal{F}_m = -\beta \int d\mathbf{r}\, Q_{ij} (\nabla_i c)(\nabla_j c) = -\beta \int d\mathbf{r} S\, (\mathbf{n} \cdot \nabla c)^2 \tag{125}$$

This captures the tendency of the director to align with the concentration gradient. Here β denotes the strength of the alignment. For $\beta > 0$ ($\beta < 0$) this favors parallel (perpendicular) alignment of the director to the gradient (see Fig. **??**A).

We consider again the nematic state with $a = -1$ and $b = 1$ so that $S = 1$ and examine the interplay between nematic elasticity K that tends to align nematigen to each other and the alignment β to a prescribed morphogen gradients $c(r) = c_0 e^{-r^2/2r_0^2}$.

By minimizing the free energy in a planar geometry starting with a perfectly aligned nematic (this is a completely passive model!) we can show that sufficiently strong alignment with the morphogen gradient can drive the unbinding of two defect pairs, as shown in Fig. 20. If we minimize the same energy on a $3d$ shape that mocks the structure of adult Hydra, with a prescribed Gaussian profile of morphogen at the head location, we recapitulate the defect structure observed in *Hydra* in vivo (see Fig. 21. More details can be found in Ref. [].

It is evident that morphogen can provide a mechanism for defect unbinding and for stabilizing defect configurations that are unstable in equilibrium such as the $+1$ defect at the head of *Hydra* [**? ?**]. Of course, it will be important to incorporate feedback between the morphogen concentration field and elasticity, where the morphogen be sourced by the stress/strain focused near topological defects [146**?**]. This is the topic of ongoing work. A more challenging direction will be develop

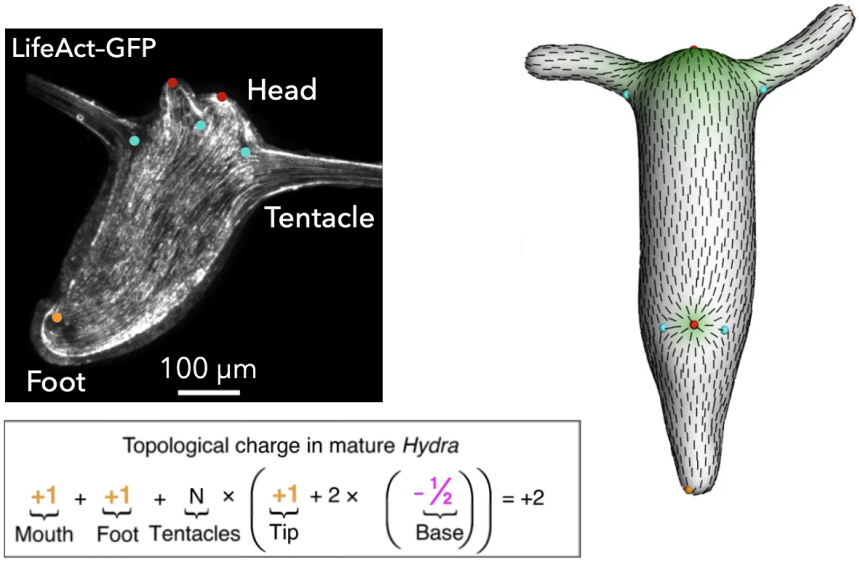

Figure 21. Left: Adult *Hydra* showing the location of topological defects (form Ref. [72]. Right: defect structure of a mock-rendering of *Hydra* with morphogen expression at the head (shown in green) highlighting the structure of topological defects. We have added a spot of Gaussian morphogen on the side of the body to display the unbinding of a $+1$ (red dot) flanked by two $-1/2$ (cyan dots) that would eventually be asosiated with the formation of a bud.

a model that incorporates the full feedback between geometry, mechanics, nematic texture and biochemical signaling, allowing for dynamical shape changes.

Finally, we note that in addition to the continuum models outlined here, there have been very interesting work on using modified vertex models on curved geometries to understand the role of nematic order and defects in *Hydra* morphogenesis.

Exercise: Derive Eq. (122) and plot a heat map of the strain.

---

[1] M Cristina Marchetti, Jean-François Joanny, Sriram Ramaswamy, Tanniemola B Liverpool, Jacques Prost, Madan Rao, and R Aditi Simha, "Hydrodynamics of soft active matter," Reviews of Modern Physics **85**, 1143 (2013).

[2] Michael te Vrugt and Raphael Wittkowski, "A review of active matter reviews," arXiv e-prints , arXiv–2405 (2024).

[3] M Cristina Marchetti, Yaouen Fily, Silke Henkes, Adam Patch, and David Yllanes, "Minimal model of active colloids highlights the role of mechanical interactions in controlling the emergent behavior of active matter," Current Opinion in Colloid & Interface Science **21**, 34–43 (2016).

[4] Michael E Cates and Julien Tailleur, "Motility-induced phase separation," Annu. Rev. Condens. Matter Phys. **6**, 219–244 (2015).

[5] Clemens Bechinger, Roberto Di Leonardo, Hartmut Löwen, Charles Reichhardt, Giorgio Volpe, and Giovanni Volpe, "Active particles in complex and crowded environments," Reviews of Modern Physics

88, 045006 (2016).
[6] Amin Doostmohammadi, Jordi Ignés-Mullol, Julia M Yeomans, and Francesc Sagués, "Active nematics," Nature communications **9**, 3246 (2018).
[7] Tim Sanchez, Daniel TN Chen, Stephen J DeCamp, Michael Heymann, and Zvonimir Dogic, "Spontaneous motion in hierarchically assembled active matter," Nature **491**, 431 (2012).
[8] Daniel Needleman, "The material basis of life," Trends in cell biology **25**, 713–716 (2015).
[9] Lakshmi Balasubramaniam, René-Marc Mège, and Benoît Ladoux, "Active nematics across scales from cytoskeleton organization to tissue morphogenesis," Current Opinion in Genetics Development **73**, 101897 (2022).
[10] Amin Doostmohammadi and Benoit Ladoux, "Physics of liquid crystals in cell biology," Trends in cell biology **32**, 140–150 (2022).
[11] Suraj Shankar, Anton Souslov, Mark J Bowick, M Cristina Marchetti, and Vincenzo Vitelli, "Topological active matter," arXiv preprint arXiv:2010.00364 (2020).
[12] Sriram Ramaswamy, "The mechanics and statistics of active matter," Annu. Rev. Condens. Matter Phys. **1**, 323–345 (2010).
[13] Michael te Vrugt, Benno Liebchen, and Michael E Cates, "What exactly is' active matter'?" arXiv preprint arXiv:2507.21621 (2025).
[14] Clemens Bechinger, Roberto Di Leonardo, Hartmut Löwen, Charles Reichhardt, Giorgio Volpe, and Giovanni Volpe, "Active particles in complex and crowded environments," Rev. Mod. Phys. **88**, 045006 (2016).
[15] Daniel Needleman and Zvonimir Dogic, "Active matter at the interface between materials science and cell biology," Nature Reviews Materials **2**, 1–14 (2017).
[16] Mark J Bowick, Nikta Fakhri, M Cristina Marchetti, and Sriram Ramaswamy, "Symmetry, thermodynamics, and topology in active matter," Physical Review X **12**, 010501 (2022).
[17] Suraj Shankar, Anton Souslov, Mark J Bowick, M Cristina Marchetti, and Vincenzo Vitelli, "Topological active matter," Nature Reviews Physics **4**, 380–398 (2022).
[18] Michael E Cates, "Diffusive transport without detailed balance in motile bacteria: does microbiology need statistical physics?" Reports on Progress in Physics **75**, 042601 (2012).
[19] Howard C Berg, *Random walks in biology* (Princeton University Press, 1993).
[20] Antoine Bricard, Jean-Baptiste Caussin, Nicolas Desreumaux, Olivier Dauchot, and Denis Bartolo, "Emergence of macroscopic directed motion in populations of motile colloids," Nature **503**, 95–98 (2013).
[21] Vishal Soni, Ephraim S Bililign, Sofia Magkiriadou, Stefano Sacanna, Denis Bartolo, Michael J Shelley, and William TM Irvine, "The odd free surface flows of a colloidal chiral fluid," Nature Physics **15**, 1188–1194 (2019).
[22] Tamás Vicsek, András Czirók, Eshel Ben-Jacob, Inon Cohen, and Ofer Shochet, "Novel type of phase transition in a system of self-driven particles," Physical Review Letters **75**, 1226 (1995).
[23] John Toner and Yuhai Tu, "Long-range order in a two-dimensional dynamical xy model: how birds fly together," Physical Review Letters **75**, 4326 (1995).
[24] Craig W Reynolds, "Flocks, herds and schools: A distributed behavioral model," in *Proceedings of the 14th annual conference on Computer graphics and interactive techniques* (1987) pp. 25–34.
[25] Ichiro Aoki, "A simulation study on the schooling mechanism in fish." NIPPON SUISAN GAKKAISHI (Bulletin of the Japanese Society of Scientific Fisheries) **48**, 1081–1088 (1982).
[26] Brian L Partridge, "The structure and function of fish schools," Scientific American **246**, 114–123 (1982).
[27] Sriram Ramaswamy and R Aditi Simha, "The mechanics of active matter: Broken-symmetry hydrodynamics of motile particles and granular layers," Solid state communications **139**, 617–622 (2006).
[28] J Prost and R Bruinsma, "Shape fluctuations of active membranes," EPL (Europhysics Letters) **33**, 321 (1996).
[29] Sriram Ramaswamy, John Toner, and Jacques Prost, "Nonequilibrium fluctuations, traveling waves, and instabilities in active membranes," Physical review letters **84**, 3494 (2000).
[30] James Darnell, Harvey Lodish, and David Baltimore, *Molecular cell biology.*, QH581. 2 D22 1990 (1990).

[31] BA Finlayson and LE Scriven, "Convective instability by active stress," Proceedings of the Royal Society of London. A. Mathematical and Physical Sciences **310**, 183–219 (1969).
[32] Robert Zwanzig, *Nonequilibrium statistical mechanics* (Oxford university press, 2001).
[33] Yaouen Fily and M Cristina Marchetti, "Athermal phase separation of self-propelled particles with no alignment," Physical review letters **108**, 235702 (2012).
[34] Gabriel S Redner, Michael F Hagan, and Aparna Baskaran, "Structure and dynamics of a phase-separating active colloidal fluid," Biophysical Journal **104**, 640a (2013).
[35] Mark J Schnitzer, "Theory of continuum random walks and application to chemotaxis," Physical Review E **48**, 2553 (1993).
[36] Julien Tailleur and Michael E Cates, "Statistical mechanics of interacting run-and-tumble bacteria," Physical review letters **100**, 218103 (2008).
[37] Claudio Maggi, Umberto Marini Bettolo Marconi, Nicoletta Gnan, and Roberto Di Leonardo, "Multidimensional stationary probability distribution for interacting active particles," Scientific reports **5**, 10742 (2015).
[38] Thomas FF Farage, Philip Krinninger, and Joseph M Brader, "Effective interactions in active brownian suspensions," Physical Review E **91**, 042310 (2015).
[39] C. Nardini, É Fodor, E. Tjhung, F. van Wijland, J. Tailleur, and M. E. Cates, "Entropy production in field theoreis without time-reversal symmetry: quantifying the non-equilibrium character of active matter," Phys. Rev. X **7**, 021007 (2017).
[40] R. Aditi Simha and Sriram Ramaswamy, "Hydrodynamic fluctuations and instabilities in ordered suspensions of self-propelled particles," Phys. Rev. Lett. **89**, 058101 (2002).
[41] Paul C Martin, Olivier Parodi, and Peter S Pershan, "Unified hydrodynamic theory for crystals, liquid crystals, and normal fluids," Physical Review A **6**, 2401 (1972).
[42] Karsten Kruse, Jean-François Joanny, Frank Jülicher, Jacques Prost, and Ken Sekimoto, "Asters, vortices, and rotating spirals in active gels of polar filaments," Physical review letters **92**, 078101 (2004).
[43] Eric Bertin, Michel Droz, and Guillaume Grégoire, "Boltzmann and hydrodynamic description for self-propelled particles," Physical Review E—Statistical, Nonlinear, and Soft Matter Physics **74**, 022101 (2006).
[44] Anton Peshkov, Eric Bertin, Francesco Ginelli, and Hugues Chaté, "Boltzmann-ginzburg-landau approach for continuous descriptions of generic vicsek-like models," The European Physical Journal Special Topics **223**, 1315–1344 (2014).
[45] David S Dean, "Langevin equation for the density of a system of interacting langevin processes," Journal of Physics A: Mathematical and General **29**, L613 (1996).
[46] Jonathan Colen, Ming Han, Rui Zhang, Steven A Redford, Linnea M Lemma, Link Morgan, Paul V Ruijgrok, Raymond Adkins, Zev Bryant, Zvonimir Dogic, *et al.*, "Machine learning active-nematic hydrodynamics," Proceedings of the National Academy of Sciences **118** (2021).
[47] Rohit Supekar, Boya Song, Alasdair Hastewell, Gary PT Choi, Alexander Mietke, and Jörn Dunkel, "Learning hydrodynamic equations for active matter from particle simulations and experiments," Proceedings of the National Academy of Sciences **120**, e2206994120 (2023).
[48] Silke Henkes, Yaouen Fily, and M Cristina Marchetti, "Active jamming: Self-propelled soft particles at high density," Physical Review E—Statistical, Nonlinear, and Soft Matter Physics **84**, 040301 (2011).
[49] Liesbeth MC Janssen, "Active glasses," Journal of Physics: Condensed Matter **31**, 503002 (2019).
[50] Dapeng Bi, Xingbo Yang, M Cristina Marchetti, and M Lisa Manning, "Motility-driven glass and jamming transitions in biological tissues," Physical Review X **6**, 021011 (2016).
[51] Elizabeth Lawson-Keister and M Lisa Manning, "Jamming and arrest of cell motion in biological tissues," Current Opinion in Cell Biology **72**, 146–155 (2021).
[52] Pasquale Digregorio, Demian Levis, Antonio Suma, Leticia F Cugliandolo, Giuseppe Gonnella, and Ignacio Pagonabarraga, "Full phase diagram of active brownian disks: from melting to motility-induced phase separation," Physical review letters **121**, 098003 (2018).
[53] Ydan Ben Dor, Yariv Kafri, and Julien Tailleur, "Forces in dry active matter," arXiv preprint

arXiv:1811.08829 (2018).
[54] Michael E Cates, D Marenduzzo, I Pagonabarraga, and J Tailleur, "Arrested phase separation in reproducing bacteria creates a generic route to pattern formation," Proceedings of the National Academy of Sciences **107**, 11715–11720 (2010).
[55] Michael E Cates and Elsen Tjhung, "Theories of binary fluid mixtures: from phase-separation kinetics to active emulsions," Journal of Fluid Mechanics **836**, P1 (2018).
[56] Joakim Stenhammar, Adriano Tiribocchi, Rosalind J Allen, Davide Marenduzzo, and Michael E Cates, "Continuum theory of phase separation kinetics for active brownian particles," Physical review letters **111**, 145702 (2013).
[57] MICHAEL E Cates, "Active field theories," Active matter and nonequilibrium statistical physics: lecture notes of the Les Houches summer school 2018 , 180–216 (2022).
[58] Elsen Tjhung, Cesare Nardini, and Michael E Cates, "Cluster phases and bubbly phase separation in active fluids: reversal of the ostwald process," Physical Review X **8**, 031080 (2018).
[59] Zhihong You, Aparna Baskaran, and M Cristina Marchetti, "Nonreciprocity as a generic route to traveling states," Proceedings of the National Academy of Sciences **117**, 19767–19772 (2020).
[60] Suropriya Saha, Jaime Agudo-Canalejo, and Ramin Golestanian, "Scalar active mixtures: The nonreciprocal cahn-hilliard model," Physical Review X **10**, 041009 (2020).
[61] Michel Fruchart, Ryo Hanai, Peter B Littlewood, and Vincenzo Vitelli, "Non-reciprocal phase transitions," Nature **592**, 363–369 (2021).
[62] Tobias Reichenbach, Mauro Mobilia, and Erwin Frey, "Mobility promotes and jeopardizes biodiversity in rock–paper–scissors games," Nature **448**, 1046–1049 (2007).
[63] Colin Scheibner, Anton Souslov, Debarghya Banerjee, Piotr Surówka, William T. M. Irvine, and Vincenzo Vitelli, "Odd elasticity," Nature Physics **16**, 475–480 (2020).
[64] Jacob Halatek, Fridtjof Brauns, and Erwin Frey, "Self-organization principles of intracellular pattern formation," Philosophical Transactions of the Royal Society B: Biological Sciences **373**, 20170107 (2018).
[65] Raphael Wittkowski, Adriano Tiribocchi, Joakim Stenhammar, Rosalind J. Allen, Davide Marenduzzo, and Michael E. Cates, "Scalar Φ4 field theory for active-particle phase separation," Nature Communications **5**, 4351 (2014).
[66] Lihong Pan and John R. de Bruyn, "Nonuniform broken-parity waves and the Eckhaus instability," Physical Review E **49**, 2119–2129 (1994).
[67] Mohammad-Ali Miri and Andrea Alù, "Exceptional points in optics and photonics," Science **363**, eaar7709 (2019).
[68] Fridtjof Brauns and M Cristina Marchetti, "Nonreciprocal pattern formation of conserved fields," Physical Review X **14**, 021014 (2024).
[69] Richard FitzHugh, "Impulses and Physiological States in Theoretical Models of Nerve Membrane," Biophysical Journal **1**, 445–466 (1961).
[70] J. Nagumo, S. Arimoto, and S. Yoshizawa, "An Active Pulse Transmission Line Simulating Nerve Axon," Proceedings of the IRE **50**, 2061–2070 (1962).
[71] Tobias Frohoff-Hülsmann and Uwe Thiele, "Nonreciprocal Cahn-Hilliard Model Emerges as a Universal Amplitude Equation," Physical Review Letters **131**, 107201 (2023).
[72] Yonit Maroudas-Sacks, Liora Garion, Lital Shani-Zerbib, Anton Livshits, Erez Braun, and Kinneret Keren, "Topological defects in the nematic order of actin fibers as organization centers of hydra morphogenesis," bioRxiv preprint bioRxiv 2020.03.02.972539 (2020).
[73] Yonit Maroudas-Sacks, Liora Garion, Lital Shani-Zerbib, Anton Livshits, Erez Braun, and Kinneret Keren, "Topological defects in the nematic order of actin fibres as organization centres of Hydra morphogenesis," Nature Physics **17**, 251–259 (2021).
[74] Yonit Maroudas-Sacks, Liora Garion, S Suganthan, Marko Popović, and Kinneret Keren, "Confinement modulates axial patterning in regenerating Hydra," bioRxiv , doi:10.1101/2024.06.13.598813 (2024).
[75] Aparna Baskaran and M Cristina Marchetti, "Hydrodynamics of self-propelled hard rods," Physical Review E—Statistical, Nonlinear, and Soft Matter Physics **77**, 011920 (2008).
[76] Suraj Shankar, Sriram Ramaswamy, and M Cristina Marchetti, "Low-noise phase of a two-dimensional

active nematic system," Physical Review E **97**, 012707 (2018).
[77] Kyogo Kawaguchi, Ryoichiro Kageyama, and Masaki Sano, "Topological defects control collective dynamics in neural progenitor cell cultures," Nature **545**, 327 (2017).
[78] Thuan Beng Saw, Amin Doostmohammadi, Vincent Nier, Leyla Kocgozlu, Sumesh Thampi, Yusuke Toyama, Philippe Marcq, Chwee Teck Lim, Julia M Yeomans, and Benoit Ladoux, "Topological defects in epithelia govern cell death and extrusion," Nature **544**, 212 (2017).
[79] Katherine Copenhagen, Ricard Alert, Ned S Wingreen, and Joshua W Shaevitz, "Topological defects promote layer formation in myxococcus xanthus colonies," Nature Physics **17**, 211–215 (2021).
[80] Oliver J Meacock, Amin Doostmohammadi, Kevin R Foster, Julia M Yeomans, and William M Durham, "Bacteria solve the problem of crowding by moving slowly," Nature Physics **17**, 205–210 (2021).
[81] Yusuf Ilker Yaman, Esin Demir, Roman Vetter, and Askin Kocabas, "Emergence of active nematics in chaining bacterial biofilms," Nature communications **10**, 1–9 (2019).
[82] Mustafa Başaran, Y Ilker Yaman, Roman Vetter, and Askin Kocabas, "Formation of self-assembled asters in growing bacterial colonies," arXiv preprint arXiv:2008.05545 (2020).
[83] R Aditi Simha and Sriram Ramaswamy, "Hydrodynamic fluctuations and instabilities in ordered suspensions of self-propelled particles," Physical review letters **89**, 058101 (2002).
[84] Luca Giomi, Mark J Bowick, Prashant Mishra, Rastko Sknepnek, and M Cristina Marchetti, "Defect dynamics in active nematics," Philosophical Transactions of the Royal Society A: Mathematical, Physical and Engineering Sciences **372**, 20130365 (2014).
[85] G Duclos, C Blanch-Mercader, V Yashunsky, G Salbreux, J-F Joanny, J Prost, and P Silberzan, "Spontaneous shear flow in confined cellular nematics," Nature physics **14**, 728 (2018).
[86] R Voituriez, Jean-François Joanny, and Jacques Prost, "Spontaneous flow transition in active polar gels," EPL (Europhysics Letters) **70**, 404 (2005).
[87] Luca Giomi, Mark J Bowick, Xu Ma, and M Cristina Marchetti, "Defect annihilation and proliferation in active nematics," Physical Review Letters **110**, 228101 (2013).
[88] Luca Giomi, "Geometry and topology of turbulence in active nematics," Physical Review X **5**, 031003 (2015).
[89] Suraj Shankar and M Cristina Marchetti, "Hydrodynamics of active defects: from order to chaos to defect ordering," Physical Review X **9**, 041047 (2019).
[90] Tyler D Ross, Heun Jin Lee, Zijie Qu, Rachel A Banks, Rob Phillips, and Matt Thomson, "Controlling organization and forces in active matter through optically defined boundaries," Nature **572**, 224–229 (2019).
[91] Rui Zhang, Steven A Redford, Paul V Ruijgrok, Nitin Kumar, Ali Mozaffari, Sasha Zemsky, Aaron R Dinner, Vincenzo Vitelli, Zev Bryant, Margaret L Gardel, *et al.*, "Spatiotemporal control of liquid crystal structure and dynamics through activity patterning," Nature Materials **20**, 875–882 (2021).
[92] LM Pismen, "Dynamics of defects in an active nematic layer," Physical Review E **88**, 050502 (2013).
[93] Ananyo Maitra and Martin Lenz, "Spontaneous rotation can stabilise ordered chiral active fluids," Nature communications **10**, 1–6 (2019).
[94] Ludwig A Hoffmann, Koen Schakenraad, Roeland MH Merks, and Luca Giomi, "Chiral stresses in nematic cell monolayers," Soft Matter (2020).
[95] Henricus H Wensink, Jörn Dunkel, Sebastian Heidenreich, Knut Drescher, Raymond E Goldstein, Hartmut Löwen, and Julia M Yeomans, "Meso-scale turbulence in living fluids," Proceedings of the National Academy of Sciences **109**, 14308–14313 (2012).
[96] Ricard Alert, Jaume Casademunt, and Jean-François Joanny, "Active turbulence," arXiv preprint arXiv:2104.02122 (2021).
[97] Suraj Shankar, Sriram Ramaswamy, M Cristina Marchetti, and Mark J Bowick, "Defect unbinding in active nematics," Physical Review Letters **121**, 108002 (2018).
[98] Shuang Zhou, Andrey Sokolov, Oleg D Lavrentovich, and Igor S Aranson, "Living liquid crystals," Proceedings of the National Academy of Sciences **111**, 1265–1270 (2014).
[99] Ewan J Hemingway, Prashant Mishra, M Cristina Marchetti, and Suzanne M Fielding, "Correlation lengths in hydrodynamic models of active nematics," Soft Matter **12**, 7943–7952 (2016).
[100] Pau Guillamat, Jordi Ignés-Mullol, and Francesc Sagués, "Taming active turbulence with patterned

soft interfaces," Nature communications **8**, 564 (2017).
[101] Linnea M Lemma, Stephen J DeCamp, Zhihong You, Luca Giomi, and Zvonimir Dogic, "Statistical properties of autonomous flows in 2d active nematics," Soft matter **15**, 3264–3272 (2019).
[102] Sumesh P Thampi, Ramin Golestanian, and Julia M Yeomans, "Velocity correlations in an active nematic," Physical review letters **111**, 118101 (2013).
[103] Felix C Keber, Etienne Loiseau, Tim Sanchez, Stephen J DeCamp, Luca Giomi, Mark J Bowick, M Cristina Marchetti, Zvonimir Dogic, and Andreas R Bausch, "Topology and dynamics of active nematic vesicles," Science **345**, 1135–1139 (2014).
[104] Diana Khoromskaia and Gareth P Alexander, "Vortex formation and dynamics of defects in active nematic shells," New Journal of Physics **19**, 103043 (2017).
[105] Dario Cortese, Jens Eggers, and Tanniemola B Liverpool, "Pair creation, motion, and annihilation of topological defects in two-dimensional nematic liquid crystals," Physical Review E **97**, 022704 (2018).
[106] Xingzhou Tang and Jonathan V Selinger, "Theory of defect motion in 2d passive and active nematic liquid crystals," Soft Matter **15**, 587–601 (2019).
[107] Yi-Heng Zhang, Markus Deserno, Zhan-Chun Tu, *et al.*, "Dynamics of active nematic defects on the surface of a sphere," Physical Review E **102**, 012607 (2020).
[108] Farzan Vafa, Mark J Bowick, M Cristina Marchetti, and Boris I Shraiman, "Multi-defect dynamics in active nematics," arXiv preprint arXiv:2007.02947 (2020).
[109] Ananyo Maitra, Martin Lenz, and Raphael Voituriez, "Chiral active hexatics: Giant number fluctuations, waves, and destruction of order," Physical Review Letters **125**, 238005 (2020).
[110] Luiza Angheluta, Zhitao Chen, M Cristina Marchetti, and Mark J Bowick, "The role of fluid flow in the dynamics of active nematic defects," New Journal of Physics **23**, 033009 (2021).
[111] Vinay Ambegaokar, BI Halperin, David R Nelson, and Eric D Siggia, "Dynamics of superfluid films," Physical Review B **21**, 1806 (1980).
[112] Annette Zippelius, BI Halperin, and David R Nelson, "Dynamics of two-dimensional melting," Physical Review B **22**, 2514 (1980).
[113] Stephen J DeCamp, Gabriel S Redner, Aparna Baskaran, Michael F Hagan, and Zvonimir Dogic, "Orientational order of motile defects in active nematics," Nature materials **14**, 1110 (2015).
[114] Elias Putzig, Gabriel S Redner, Arvind Baskaran, and Aparna Baskaran, "Instabilities, defects, and defect ordering in an overdamped active nematic," Soft Matter **12**, 3854–3859 (2016).
[115] Pragya Srivastava, Prashant Mishra, and M Cristina Marchetti, "Negative stiffness and modulated states in active nematics," Soft matter **12**, 8214–8225 (2016).
[116] Aurelio Patelli, Ilyas Djafer-Cherif, Igor S Aranson, Eric Bertin, and Hugues Chaté, "Understanding dense active nematics from microscopic models," Physical review letters **123**, 258001 (2019).
[117] Amin Doostmohammadi, Michael F Adamer, Sumesh P Thampi, and Julia M Yeomans, "Stabilization of active matter by flow-vortex lattices and defect ordering," Nature communications **7**, 10557 (2016).
[118] Anand U Oza and Jörn Dunkel, "Antipolar ordering of topological defects in active liquid crystals," New Journal of Physics **18**, 093006 (2016).
[119] DJG Pearce, J Nambisan, PW Ellis, Z Dogic, A Fernandez-Nieves, and L Giomi, "Scale-free defect ordering in passive and active nematics," arXiv preprint arXiv:2004.13704 (2020).
[120] Kristian Thijssen, Mehrana R Nejad, and Julia M Yeomans, "Role of friction in multidefect ordering," Physical Review Letters **125**, 218004 (2020).
[121] Mark Warner and Eugene Terentjev, *Liquid Crystal Elastomers*, International Series of Monographs on Physics No. 120 (Clarendon Press, Oxford, 2003).
[122] Laurens T. de Haan, Carlos Sánchez-Somolinos, Cees M. W. Bastiaansen, Albertus P. H. J. Schenning, and Dirk J. Broer, "Engineering of Complex Order and the Macroscopic Deformation of Liquid Crystal Polymer Networks," Angewandte Chemie **124**, 12637–12640 (2012).
[123] Mark Warner, "Topographic Mechanics and Applications of Liquid Crystalline Solids," Annual Review of Condensed Matter Physics **11**, 125–145 (2020).
[124] C. D. Modes, K. Bhattacharya, and M. Warner, "Gaussian curvature from flat elastica sheets," Proceedings of the Royal Society A: Mathematical, Physical and Engineering Sciences **467**, 1121–1140 (2011).
[125] Cyrus Mostajeran, "Curvature generation in nematic surfaces," Physical Review E **91**, 062405 (2015).

[126] Daniel Duffy and John S. Biggins, "Defective nematogenesis: Gauss curvature in programmable shape-responsive sheets with topological defects," Soft Matter **16**, 10935–10945 (2020).
[127] Diana Khoromskaia and Guillaume Salbreux, "Active morphogenesis of patterned epithelial shells," eLife **12**, e75878 (2023).
[128] Alan M. Turing, "The chemical basis of morphogenesis," Philosophical Transactions of the Royal Society of London. Series B, Biological Sciences **237**, 37–72 (1952).
[129] L. Wolpert, "Positional information and the spatial pattern of cellular differentiation," Journal of Theoretical Biology **25**, 1–47 (1969).
[130] Angelika Böttger and Monika Hassel, "Hydra, a model system to trace the emergence of boundaries in developing eumetazoans," The International Journal of Developmental Biology **56**, 583–591 (2012).
[131] Rui Wang, Robert E. Steele, and Eva-Maria S. Collins, "Wnt signaling determines body axis polarity in regenerating Hydra tissue fragments," Developmental Biology **467**, 88–94 (2020).
[132] Lital Shani-Zerbib, Liora Garion, Yonit Maroudas-Sacks, Erez Braun, and Kinneret Keren, "Canalized Morphogenesis Driven by Inherited Tissue Asymmetries in Hydra Regeneration," Genes **13**, 360 (2022).
[133] Joann J. Otto, "Orientation and behavior of epithelial cell muscle processes duringHydra budding," Journal of Experimental Zoology **202**, 307–321 (1977).
[134] I. Philipp, R. Aufschnaiter, S. Ozbek, S. Pontasch, M. Jenewein, H. Watanabe, F. Rentzsch, T. W. Holstein, and B. Hobmayer, "Wnt/β-Catenin and noncanonical Wnt signaling interact in tissue evagination in the simple eumetazoan *Hydra*," Proceedings of the National Academy of Sciences **106**, 4290–4295 (2009).
[135] Roland Aufschnaiter, Roland Wedlich-Söldner, Xiaoming Zhang, and Bert Hobmayer, "Apical and basal epitheliomuscular F-actin dynamics during *Hydra* bud evagination," Biology Open **8**, bio.022723 (2017).
[136] T. C. Lubensky, Ranjan Mukhopadhyay, Leo Radzihovsky, and Xiangjun Xing, "Symmetries and elasticity of nematic gels," Physical Review E **66**, 011702 (2002).
[137] Kyogo Kawaguchi, Ryoichiro Kageyama, and Masaki Sano, "Topological defects control collective dynamics in neural progenitor cell cultures," Nature **545**, 327–331 (2017).
[138] Lakshmi Balasubramaniam, Amin Doostmohammadi, Thuan Beng Saw, Gautham Hari Narayana Sankara Narayana, Romain Mueller, Tien Dang, Minnah Thomas, Shafali Gupta, Surabhi Sonam, Alpha S Yap, *et al.*, "Investigating the nature of active forces in tissues reveals how contractile cells can form extensile monolayers," Nature materials , 1–11 (2021).
[139] Farzan Vafa, Mark J Bowick, Boris I Shraiman, and M Cristina Marchetti, "Fluctuations can induce local nematic order and extensile stress in monolayers of motile cells," Soft Matter **17**, 3068–3073 (2021).
[140] Andrew Killeen, Thibault Bertrand, and Chiu Fan Lee, "Polar fluctuations lead to extensile nematic behavior in confluent tissues," Physical Review Letters **128**, 078001 (2022).
[141] Lasse Bonn, Aleksandra Ardaševa, Romain Mueller, Tyler N Shendruk, and Amin Doostmohammadi, "Fluctuation-induced dynamics of nematic topological defects," Physical Review E **106**, 044706 (2022).
[142] Mathieu Dedenon and Karsten Kruse, "Noise-induced transitions from contractile to extensile active stress in isotropic fluids," arXiv preprint arXiv:2410.14358 (2024).
[143] Mehrana R Nejad, Liam J Ruske, Molly McCord, Jun Zhang, Guanming Zhang, Jacob Notbohm, and Julia M Yeomans, "Stress-shape misalignment in confluent cell layers," Nature Communications **15**, 3628 (2024).
[144] Pradip K. Bera, Molly McCord, Jun Zhang, and Jacob Notbohm, "Energy Dynamics Powered by Traction and Stress Control Formation and Motion of +1/2 Topological Defects in Epithelial Cell Monolayers," arXiv , arXiv:2501.04827 (2025), arXiv:2501.04827 [physics].
[145] Pau Guillamat, Waleed Mirza, Pradeep K. Bal, Manuel Gómez-González, Pere Roca-Cusachs, Marino Arroyo, and Xavier Trepat, "Guidance of cellular nematics into shape-programmable living surfaces," bioRxiv (2025), 10.1101/2025.06.27.660992.
[146] Jaroslav Ferenc, Panagiotis Papasaikas, Jacqueline Ferralli, Yukio Nakamura, Sebastien Smallwood, and Charisios D. Tsiairis, "Wnt3 expression as a readout of tissue stretching during *Hydra* regenera-

tion," bioRxiv , doi:10.1101/2020.12.22.423911 (2020).